Relativistic Transport Approach for Nucleus-Nucleus Collisions based on a NJL Lagrangian ⋆,⋆⋆

W. Ehehalt and W. Cassing

Institut für Theoretische Physik, Universität Giessen, 35392 Giessen, Germany

Abstract

We formulate a covariant transport approach for high energy nucleus-nucleus collisions where the real part of the hadron selfenergies is evaluated on the basis of a NJL-type Lagrangian for the quark degrees of freedom. The parameters of the model Lagrangian are fixed by the Gell-Mann, Oakes and Renner relation, the pion-nucleon Σ-term, the nucleon energy as well as the nuclear binding energy at saturation density ρ_0. We find the resulting scalar and vector selfenergies for nucleons to be well in line with either Dirac-Brueckner results or those from the phenomenological optical potential when accounting for a swelling of the nucleon at finite nuclear matter density. The imaginary part of the hadron selfenergies is determined by a string fragmentation model which accounts for the in-medium mass of hadrons in line with the chiral dynamics employed. The applicability of the 'chiral' transport approach is demonstrated in comparison with experimental data from SIS to SPS energies. The enhancement of the K^+/π^+ ratio in A + A collisions compared to p + A reactions at AGS energies is reproduced within the 'chiral' dynamics. Furthermore, detailed predictions for the stopping in Pb + Pb collisions at 153 GeV/A are presented.

1 Introduction

The study of hot and dense nuclear matter by means of relativistic nucleus-nucleus collisions is the major aim of high energy heavy-ion physics. However, any conclusions about the nuclear properties at high temperature or baryon densities must rely on the comparison of experimental data with theoretical approaches based on nonequilibrium kinetic theory. Among these, the covariant RBUU approach [1–9], the QMD [10] or RQMD model [11] have been

⋆ supported by DFG and GSI Darmstadt
⋆⋆ Part of the PhD thesis of W. Ehehalt

successfully used in the past. As a genuine feature of transport theories there are two essential ingredients: i.e. the baryon (and meson) scalar and vector selfenergies - which are neglected in a couple of approaches - as well as in-medium elastic and inelastic cross sections for all hadrons involved. Whereas in the low-energy regime these 'transport coefficients' can be calculated in the Dirac-Brueckner approach starting from the bare nucleon-nucleon interaction [12,13], this is no longer possible at high baryon density ($\rho_B \leq$ 2-3ρ_0) and high temperature, since the number of independent hadronic degrees of freedom increases drastically and the nuclear system is expected to enter a phase where chiral symmetry is restored [14–17]. Such a phase transition is dynamically due to a change of the nonperturbative QCD vacuum at high temperature or baryon density and the chiral invariance of the interaction between quarks and gluons in the QCD Lagrangian. As a consequence the hadron selfenergies in the nuclear medium should change substantially especially close to the chiral phase transition and any transport theoretical study should include the generic properties of QCD that so far are known from nonperturbative computations on the lattice [18–21]. However, such nonperturbative calculations will not be possible for high baryon densities within the next years and we have to rely on suitable effective Lagrangians that lead to the same physical condensates and thermodynamic behaviour as the original QCD problem.

Our approach thus first aims at fixing an effective Lagrangian for the quark degrees of freedom on the mean-field (one loop) level for low energy QCD problems where the gluon fields $A^a_\mu(x)$ have been integrated out. The effective interaction determined in this way should not be used in further perturbation theory (e.g. for scattering or transition rates) since it is supposed to be the result of an infinite resummation of interaction diagrams. In the first step of this work we aim at fixing the real part of the quark selfenergy - that determines the properties of the system in thermodynamic equilibrium - and in a second step then extract the real part of nucleon selfenergies from quark configurations that describe nuclear matter at finite density. In a third step then the imaginary part of the hadron selfenergies - or their collision rates - will be specified within an extended LUND string model.

Our primary strategy is similar to that of Skyrme forces [22] in the nonrelativistic nuclear physics context or that of the σ-ω model for a relativistic description of finite nuclei and nuclear matter [23]. In fact, it will turn out that the present approach leads to nucleon selfenergies quite close to those from the σ-ω model [24] for the nucleons.

The underlying idea of an effective 4-point interaction for quarks has already been discussed e.g. by Vogl and Weise in ref. [25]. Since the fundamental currents in QCD are color currents, i.e. $J^a_\mu = \bar{\psi}_q \gamma_\mu t^a \psi_q$, an elementary color current interaction with a universal coupling G_C is expected to be dominant.

An effective Lagrangian for $\delta(x_1 - x_2)$-like quark interactions thus reads

$$L_{\rm q}(x) = \bar{\psi}_{\rm q}({\rm i}\gamma^\mu\partial_\mu - \hat{m}_0)\psi_{\rm q} - G_{\rm C}^2 \sum_{a=1}^{8} \left(\bar{\psi}_{\rm q}\gamma_\mu t^a \psi_{\rm q}\right)^2 , \tag{1}$$

where $t^a (a = 1, ..., 8)$ are the $SU(3)_{\rm color}$ matrices with $tr(t^a t^b) = \delta_{ab}/2, \hat{m}_0$ a diagonal mass matrix in flavor space, i.e. $\hat{m}_0 = diag(m_{\rm u}^0, m_{\rm d}^0, m_{\rm s}^0)$ and $\bar{\psi}_{\rm q} = (\bar{\rm u}, \bar{\rm d}, \bar{\rm s})$ is the quark spinor in case of $SU(3)_{\rm flavor}$. The color-current interaction is invariant under chiral transformations or $SU(3)_{\rm flavor}$ rotations. The Lagrangian (1), however, in its present form is not yet well suited for the formulation of quark dynamics on the mean-field level because antisymmetrization generates a further mixing of color, flavor and Dirac indices. It is thus more convenient to introduce a Fierz transformation, i.e. to antisymmetrize the 4-point interaction to proceed with further computations on the Hartree level. The Fierz transform then generates color singlet as well as color octet terms, i.e. [25,26]

$$\begin{aligned}
L_{\rm q}(x) = {} & \bar{\psi}_{\rm q}({\rm i}\gamma^\mu\partial_\mu - \hat{m}_0)\psi_{\rm q} + G_{\rm S}^2 \sum_{i=0}^{8} \left\{ \left(\bar{\psi}_{\rm q}\frac{\lambda_i}{2}\psi_{\rm q}\right)^2 + \left(\bar{\psi}_{\rm q}{\rm i}\gamma_5\frac{\lambda_i}{2}\psi_{\rm q}\right)^2 \right\} \\
& - G_{\rm V}^2 \sum_{i=0}^{8} \left\{ \left(\bar{\psi}_{\rm q}\gamma_\mu\frac{\lambda_i}{2}\psi_{\rm q}\right)^2 + \left(\bar{\psi}_{\rm q}\gamma_5\gamma^\mu\frac{\lambda_i}{2}\psi_{\rm q}\right)^2 \right\} \\
& - G_{\rm C}^2 \sum_{a=1}^{8} \left(\bar{\psi}_{\rm q}\gamma_\mu t^a\psi_{\rm q}\right)^2 - \frac{2}{3}G_{\rm C}^2 \sum_{a=1}^{8}\sum_{i=0}^{8} \left\{ \left(\bar{\psi}_{\rm q}\frac{\lambda^i}{2}t^a\psi_{\rm q}\right)^2 + \left(\bar{\psi}_{\rm q}{\rm i}\gamma_5\frac{\lambda^i}{2}t^a\psi_{\rm q}\right)^2 \right\} \\
& + \frac{1}{3}G_{\rm C}^2 \sum_{a=1}^{8}\sum_{i=0}^{8} \left\{ \left(\bar{\psi}_{\rm q}\gamma_\mu\frac{\lambda^i}{2}t^a\psi_{\rm q}\right)^2 + \left(\bar{\psi}_{\rm q}\gamma_\mu\gamma_5\frac{\lambda^i}{2}t^a\psi_{\rm q}\right)^2 \right\} ,
\end{aligned} \tag{2}$$

where $G_{\rm S}^2 = 2G_{\rm V}^2 = \frac{8}{9}G_{\rm C}^2$. In (2) the matrices $\lambda^i (i = 1, .., 8)$ stand for the $SU(3)_{\rm flavor}$ degrees of freedom with $tr(\lambda_i\lambda_j) = 2\delta_{ij}$ while λ^0 is given by $\lambda^0 = \sqrt{\frac{2}{3}}I_3$ with I_3 denoting the 3x3 unitary matrix in flavor space[1] . The Lagrangian (2) in its color-singlet version has been the starting point for RPA-type calculations for the bosonic excitations of the nonperturbative QCD vacuum, i.e. the mesonic degrees of freedom [25–27]. Similar Lagrangian densities have also been exploited by a variety of authors [28–36] following an early suggestion by Nambu and Jona-Lasinio (NJL) [37].

In our present study we will discard the mesonic (RPA-type) sector and concentrate on the determination of an effective quark-quark interaction by nu-

[1] The most general four-point interaction compatible with QCD symmetries starts from combinations of all possible vector and axial currents. Therefore, in general, there is no strict relationship between $G_{\rm S}$ and $G_{\rm V}$.

cleon properties as well as nuclear matter related quantities. Similar concepts have been proposed by Guichon [38] and Saito and Thomas [39] based on bag-model wavefunctions. Here we start with a slightly different strategy by determining the free quark wavefunctions from the experimental data for the proton electromagnetic formfactor. In this way we intend to circumvent the problem of absolute confinement which cannot be dealt with properly using only a color neutral mean-field approach of the NJL-type.

Qur work is organized as follows: In Section 2 we will fix the free parameters of our model interaction by the Gell-Mann, Oakes and Renner relation [40], the pion-nucleon Σ-term and the free 'nucleon' mass. In Section 3 we will then extend our study to the computation of the energy density of nuclear matter configurations, discuss the necessary modification of the nucleon formfactor in the medium and present results for the proton-nucleus optical potential as a function of the laboratory kinetic energy at normal nuclear matter density ρ_0. We, furthermore, compare our results to the low density, low energy Dirac phenomenology and point out the open problems. In Section 4 we specify the modifications of the familiar LUND string-fragmentation model [41], which models the imaginary part of the hadron selfenergies, to include (as a first step) the modification of the hadron masses at finite baryon density. In Section 5 we apply our transport approach to nucleus-nucleus collisions from SIS to SPS energies and test its applicability in comparison with experimental data. Section 6, finally, is devoted to a summary and discussion of open problems.

2 The isospin symmetric nucleon system

In this Section we concentrate on vacuum as well as nucleon properties where the nucleons are assumed to be represented by 3 additional valence quarks on top of the (truncated) Dirac-sea with a formfactor in line with the experimental data. The singlet terms of the Lagrangian (2) in the mean-field limit - performing the sum over the flavor matrix elements - then leads to the following Lagrangian for $\bar{\psi}_k = (\bar{\mathrm{u}}, \bar{\mathrm{d}}, \bar{\mathrm{s}})$,

$$
\begin{aligned}
L_{\mathrm{q}}(x) = & \sum_{k=\mathrm{u,d,s}} \left\{ \bar{\psi}_k \left(\mathrm{i}\gamma^\mu \partial_\mu - m_k^0 \right) \psi_k \right. \\
& + \frac{G_{\mathrm{S}}^2}{2} \left\{ \left(\bar{\psi}_k \psi_k \right)^2 + \left(\bar{\psi}_k \mathrm{i}\gamma_5 \psi_k \right)^2 \right\} \\
& \left. - \frac{G_{\mathrm{V}}^2}{2} \left\{ \left(\bar{\psi}_k \gamma_\mu \psi_k \right)^2 + \left(\bar{\psi}_k \gamma_5 \gamma^\mu \psi_k \right)^2 \right\} \right\} , \qquad (3)
\end{aligned}
$$

where the couplings G_{S}^2 and G_{V}^2 are now considered as free parameters. For the systems of positive parity, which are of interest in our present work, also

the pseudoscalar and pseudovector terms vanish in the Hartree limit such that we are left with the scalar and vector term, only. This is quite similar to the σ-ω model [23] in the nuclear physics context. The hamiltonian density then is given by

$$\mathcal{H}(x) = \sum_{k=\mathrm{u,d,s}} \Big\{ \bar{\psi}_k \left(-\mathrm{i}\gamma^i \partial_i + m_k^0 - G_\mathrm{S}^2 \langle \bar{\psi}_k \psi_k \rangle \right) \psi_k + \frac{G_\mathrm{S}^2}{2} \langle \bar{\psi}_k \psi_k \rangle^2 + \frac{G_\mathrm{V}^2}{2} \langle \bar{\psi}_k \gamma_\mu \psi_k \rangle^2 \Big\}, \tag{4}$$

which leads to the gap equations for the effective masses m_k, i.e.

$$m_k = m_k^0 - G_\mathrm{S}^2 \langle \bar{\psi}_k \psi_k \rangle. \tag{5}$$

Since the problem (4) decouples in the flavor degrees of freedom we will consider in the following only u-quarks assuming $m_\mathrm{u}^0 = m_\mathrm{d}^0$ and neglect a possible strangeness content of the nucleon furtheron.

For the nonperturbative vacuum we then end up with the gap equation in phase space for the effective quark mass m_u of u or d quarks:

$$m_\mathrm{u} = m_\mathrm{u}^0 + G_\mathrm{S}^2 \frac{g}{(2\pi)^3} \int d^3p \frac{m_\mathrm{u}}{\sqrt{p^2 + m_\mathrm{u}^2}} \, \Theta(\Lambda_\mathrm{S} - \mid \mathbf{p} \mid) = m_V^* \tag{6}$$

where we have introduced an euclidian cutoff parameter Λ_S to regularize the divergent integral over the Dirac sea. Alternatively, one might also introduce covariant cutoff schemes as in [25,34], but for reasons to discussed below in context of eq. (8) we prefer to use the euclidian scheme, since we are basically interested in quark configurations with a well defined rest frame. In eq. (6) the factor $g = 6$ arizes from the trace over color and spin in eq. (5). The gap equation (6) then leads to a constituent quark mass $m_\mathrm{u} > m_\mathrm{u}^0$ in the nonperturbative vacuum.

The coupling constant G_S together with the cutoff parameter Λ_S now can be determined via the Gell-Mann, Oakes and Renner relation [40] assuming $\langle \bar{\mathrm{u}}\mathrm{u} \rangle = \langle \bar{\mathrm{d}}\mathrm{d} \rangle$,

$$m_\pi^2 \, f_\pi^2 = -(m_\mathrm{u}^0 + m_\mathrm{d}^0) \, \langle \bar{\mathrm{u}}\mathrm{u} \rangle \ , \tag{7}$$

where $f_\pi = 93.3$ MeV is the pion decay constant, m_π the physical pion mass and $\langle \bar{\mathrm{u}}\mathrm{u} \rangle$ the scalar condensate (for u or d quarks in the vakuum). Choosing $m_\mathrm{u}^0 = 7$ MeV as an average value of the light quark mass the quark condensate then amounts to $\langle \bar{\mathrm{u}}\mathrm{u} \rangle^{1/3} \approx -230$ MeV; a value which is achieved by choosing a cutoff $\Lambda_\mathrm{S} \approx 0.59$ GeV and $G_\mathrm{S} \approx 4.95$ GeV^{-1} in (6).

In the presense of additional localized light valence quarks on top of the Dirac sea the gap equation (6) modifies locally to

$$m_{\rm u}(\mathbf{r}) = m_{\rm u}^0 - G_{\rm S}^2 \frac{g}{(2\pi)^3} \int d^3p \frac{m_{\rm u}(\mathbf{r})}{\sqrt{p^2 + m_{\rm u}(\mathbf{r})^2}}\ f_{\rm u}(\mathbf{r},\mathbf{p})$$
$$+G_{\rm S}^2 \frac{g}{(2\pi)^3} \int \frac{m_{\rm u}(\mathbf{r})}{\sqrt{p^2 + m_{\rm u}(\mathbf{r})^2}}\ \Theta(\Lambda_{\rm S} - \mid \mathbf{p} \mid), \tag{8}$$

where $f_{\rm u}(\mathbf{r},\mathbf{p})$ denotes the phase-space distribution of a single u-quark which has to determined in a model dependent way.

In view of an implementation in a transport theory this expression now is evaluated in the local density approximation for $f_{\rm u}(\mathbf{r},\mathbf{p})$ on the basis of the experimental electromagnetic formfactor of the proton which is well represented by a dipole approximation even up to momentum transfers $Q^2 \approx 25$ GeV^2/c^2 [42]. This implies that the quark charge distribution (of a proton) is of the exponential form [43]

$$\langle \psi_{\rm q}^\dagger(\mathbf{r}) \psi_{\rm q}(\mathbf{r}) \rangle \approx N_0\ exp(- \mid \mathbf{r} \mid /b_0) = \rho_{\rm q}(\mathbf{r}), \tag{9}$$

where $\mathbf{r}$ is given in fm, $b_0 = 0.25$ fm and $N_0 = (8\pi r_0^3)^{-1}$ provides normalization to 1. Considering now a nucleon state averaged over spin and isospin, i.e. a mixture of proton, neutron and Δ's of average mass $M_{\rm N} \approx 1.085$ GeV, we obtain for the u-quark density

$$\rho_{\rm u}(\mathbf{r}) \approx \frac{3}{2} N_0\ exp(- \mid \mathbf{r} \mid /b_0), \tag{10}$$

where the factor 3/2 reflects the average u-quark content of the states considered. In the local density approximation the phase-space distribution for u-quarks then is given by

$$f_{\rm u}(\mathbf{r},\mathbf{p}) = \Theta(p_{\rm F}(\mathbf{r}) - \mid \mathbf{p} \mid) \tag{11}$$

with the local Fermi momentum

$$p_{\rm F}(\mathbf{r}) = (6/g\ \pi^2)^{1/3} \rho_{\rm u}(\mathbf{r})^{1/3}. \tag{12}$$

This approximation has been quite successfully applied in the nuclear physics context [1,2] and also been adopted in [44,45] for quark oriented models. It is a legitimate approximation for the quark phase-space distribution as long as one is interested in expectation values like the total energy, only.

The coordinate-space dependence of $m_{\rm u}(\mathbf{r})$ (full line) for the nucleon is shown in Fig. 1 together with the u-quark density $\langle {\rm u}^\dagger(r){\rm u}(r)\rangle = \rho_{\rm u}(r)$. In the interior

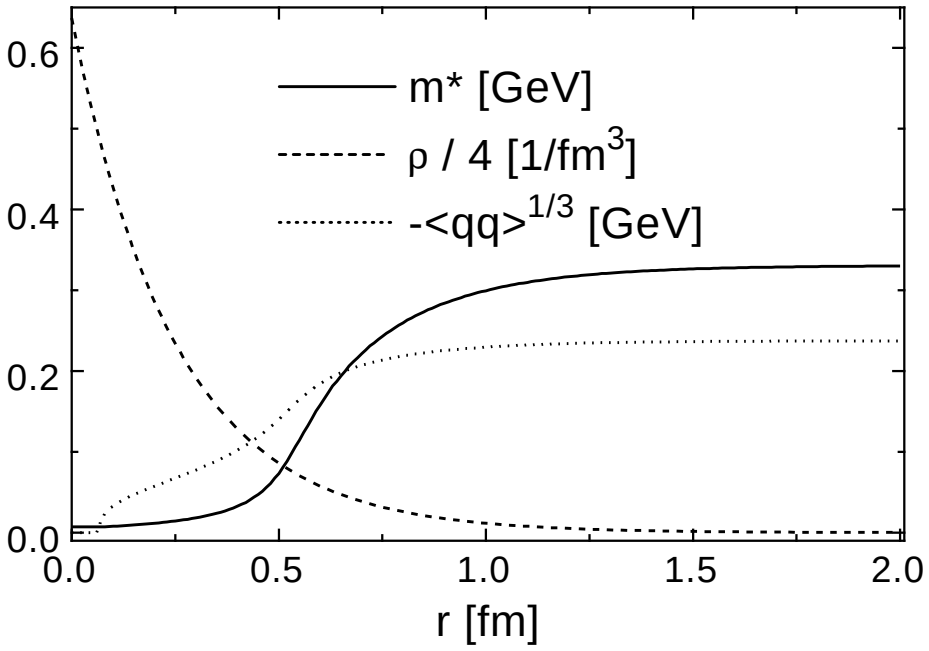

Fig. 1. Effective mass m^* (full line), quark density (dashed line) and scalar condensate $-<\bar{q}q>^{1/3}$ (dotted line) as a function of the radial distance from the quark center.

of the nucleon the effective quark mass drops to about $m_{\rm u}^0 = 7$ MeV and thus the quark scalar selfenergy $U_{\rm S}$ to zero.

The energy density $T^{00}(\mathbf{r})$ - for the average nucleon system considered - in phase-space representation reads (including a factor of 2 from the summation over u and d quarks)

$$
\begin{aligned}
T^{00}(\mathbf{r}) &= 2g \int \frac{d^3p}{(2\pi)^3} \sqrt{p^2 + m_{\rm u}(\mathbf{r})^2}\ f(\mathbf{r},\mathbf{p}) \\
&-2g \int \frac{d^3p}{(2\pi)^3} \sqrt{p^2 + m_{\rm u}(\mathbf{r})^2}\ \Theta(\Lambda_{\rm S} - \mid \mathbf{p} \mid) \\
&+2\left\{ \frac{1}{2} G_{\rm S}^2 \rho_{\rm S}(\mathbf{r})^2 + \frac{1}{2} G_{\rm V}^2 \rho_V(\mathbf{r})^2 \right\} - E_{\rm vac}
\end{aligned}
\tag{13}
$$

where the vacuum contribution

$$
E_{\rm vac} = -2\left\{ g \int \frac{d^3p}{(2\pi)^3} \sqrt{p^2 + m_{\rm u}^2}\ \Theta(\Lambda_{\rm S} - \mid \mathbf{p} \mid) + \frac{1}{2} G_{\rm S}^2 \rho_{\rm S0}^2 \right\}
\tag{14}
$$

has been subtracted. $\rho_{\rm S} = (m - m^0)/G_{\rm S}^2$ is the scalar density and $\rho_{\rm V} = \frac{g}{(2\pi)^3}\int d^3p\ f_u(\mathbf{r},\mathbf{p})$ the vector density. The total energy $\langle H\rangle$ of a quark configuration described by $f_{\rm u}(\mathbf{r},\mathbf{p})$ then is obtained by integrating $\int d^3r\ T^{00}(\mathbf{r})$.

The average nucleon energy to be fixed in our case corresponds to 1.085 GeV, which is the average of the nucleon and the Δ mass. Our fit provides $G_{\rm V} = 4.2$ GeV^{-1} for the total energy of a nucleon using $f_{\rm u}(\mathbf{r},\mathbf{p}) = \Theta(p_{\rm F}(\mathbf{r}) - \mid \mathbf{p} \mid)$ with $p_{\rm F}(\mathbf{r})$ from (12). The pion-nucleon Σ-term, defined by the following matix elements with the nucleon state,

$$\Sigma_{\pi{\rm N}} = \frac{1}{2}(m_{\rm u}^0 + m_{\rm d}^0)\ \langle {\rm N}|\bar{\rm u}{\rm u} + \bar{\rm d}{\rm d}|{\rm N}\rangle\ , \tag{15}$$

within the parameters stated above leads to $\Sigma_{\pi{\rm N}} \approx 47$ MeV which is well in line with the value extracted from pion-nucleon s-wave scattering of 45 ± 7 MeV from [46].

3 Symmetric nuclear matter

In order to evaluate the energy density for symmetric nuclear matter configurations we have to introduce in addition to $f_{\rm q} = f_{\rm u}(\mathbf{r},\mathbf{p})$ a phase-space distribution for the nucleons or 'localized' quark states $f_{\rm N}$. Denoting by $(\mathbf{r}_{\rm N},\mathbf{p}_{\rm N})$ the position and momentum of a nucleon, the corresponding quark phase-space distribution $f_{\rm q}(\mathbf{r},\mathbf{p})_{\mathbf{r}_{\rm N},\mathbf{p}_{\rm N}}$ is obtained from a translation of the center of $f_{\rm q}$ by $\mathbf{r}_{\rm N}$ and a proper Lorentz transformation by $\beta_{\rm N} = \mathbf{p}/\sqrt{p^2 + m_{\rm N}^2}$ in phase space, i.e. a contraction of $f_{\rm q}$ by $\gamma_{\rm N}^{-1} = \sqrt{1-\beta_{\rm N}^2}$ in coordinate space and dilation in momentum space by $\gamma_{\rm N}$, which keeps the individual phase space integral invariant.

As an example the local quark phase-space distribution $f_{\rm u}(\mathbf{r},\mathbf{p})$ - as met in the overlap regime of two colliding quark states - is depicted in Fig. 2 as a function of p_x and p_z for $p_y = 0$. It's macroscopic parameters are given by the relative momenta P_1, P_2 of the 'quark wave functions' with respect to the nuclear matter rest frame and the individual Fermi momenta $p_{\rm F1}(\mathbf{r}), p_{\rm F2}(\mathbf{r})$ that are determined by the individual densities at space position $\mathbf{r}$ by $p_{\rm F}(\mathbf{r}) = (6g\pi^2\rho_{\rm q}^i(\mathbf{r}))^{1/3}$ as before. The Dirac sea contribution is indicated by the sphere with radius $\Lambda_{\rm S}$.

Iteration of the gap equation (8) then yields the effective mass $m(\mathbf{r};P_1,P_2,\rho^1,\rho^2)$ as well as the scalar density $\rho_{\rm S}(\mathbf{r})$. The resulting quark vector (solid lines) and scalar densities (dashed lines) are displayed in Fig. 3 as a function of $z = r$ for $x = y = 0$ for different distances R of the two nucleons (and a constant

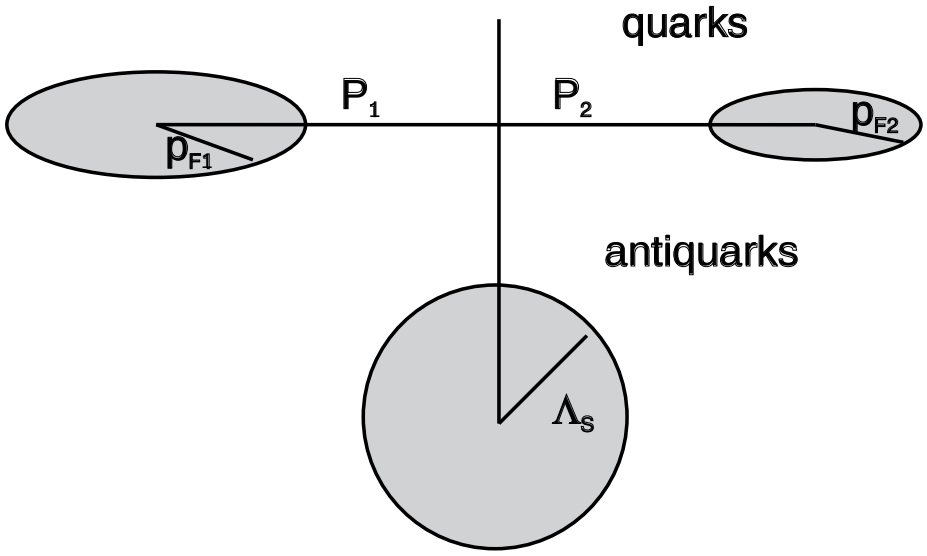

Fig. 2. Characteristic quark phase-space distribution in the overlap regime for two colliding nucleons for $p_y = 0$. The sphere with radius Λ_S characterizes the Dirac sea contribution at rest.

relative momentum $P = 0.2$ GeV/c). Due to the gap equation (8) the scalar quark density drops substantially even for a moderate overlap of the nucleons ($R \approx 1.6$fm), which reflects the 'intermediate' range (σ-field) attraction of the two nucleons, whereas the overlap of the vector densities becomes more substantial at short distance ($R \approx 0.5$fm), which reflects the ω-field in terms of the conventional σ-ω model [23].

For isospin symmetric nuclear matter the nucleon phase-space distribution for fixed spin and isospin is given by

$$f_{\rm N}(\mathbf{r}_{\rm N}, \mathbf{p}_{\rm N}) = \Theta(p_{\rm F} - \mid \mathbf{p}_{\rm N} \mid) \tag{16}$$

with the nucleon Fermi momentum given by $p_{\rm F} = (6/4\pi^2\rho_{\rm N})^{1/3}$ where $\rho_{\rm N}$ is the nuclear matter density which will be discussed in units of $\rho_0 \approx 0.17$ fm^{-3}. In addition, the 'localized wave packets' move with individual momenta $\mathbf{p}_{\rm N}$ that are selected by Monte Carlo with the constraint $\mid \mathbf{p}_{\rm N} \mid \leq p_{\rm F}$. The nucleon

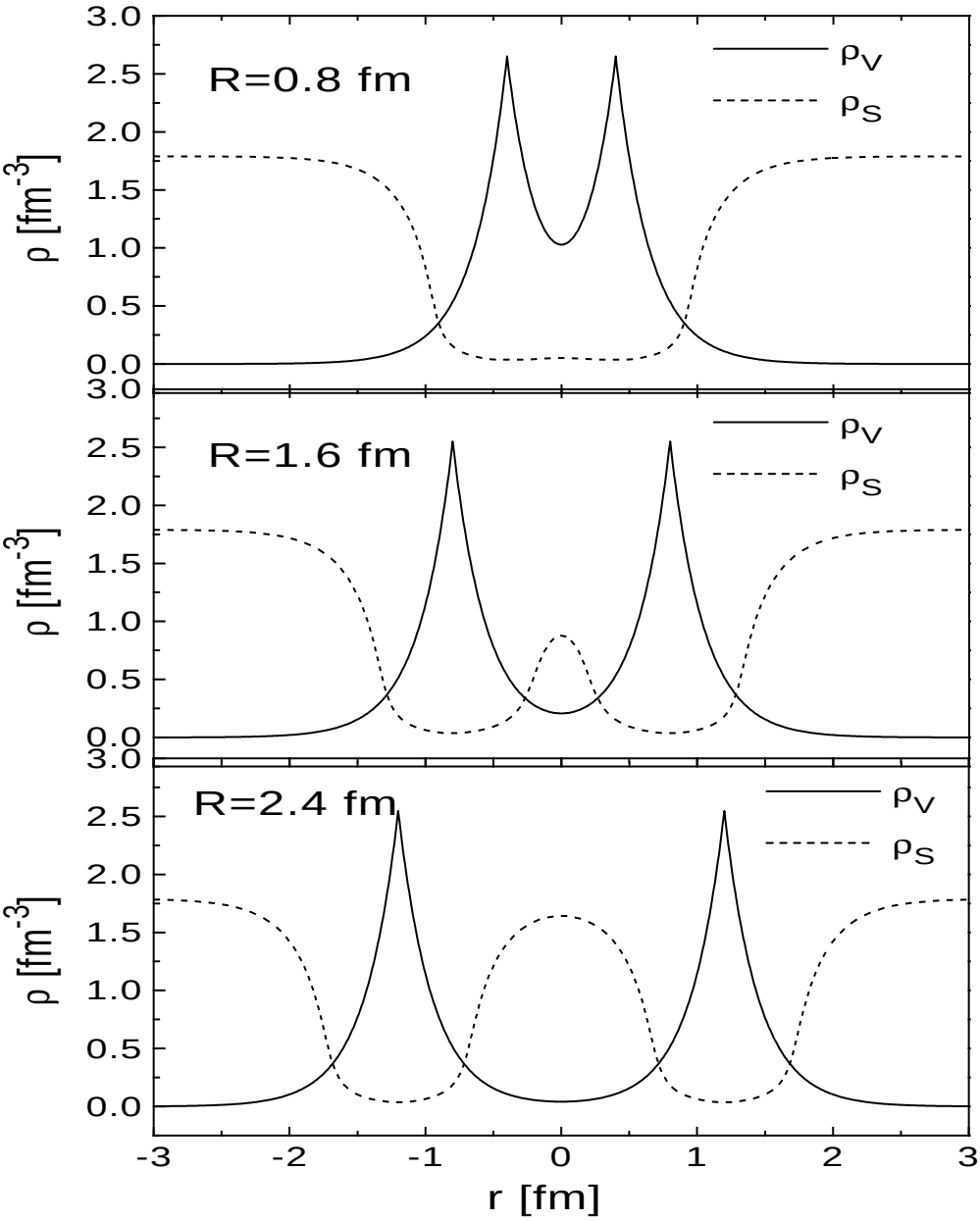

Fig. 3. Spatial quark distribution (full lines) and scalar quark density (dashed lines) for two colliding nucleons with relative momentum $P = 0.2$ GeV/c for different relative distances R from 0.8 fm to 2.4 fm.

phase-space distribution is generated by Monte Carlo for 64 nucleons in a unit volume ($a = 1$ fm, $p_{\rm F} = 1$ fm^{-1}) and the density dependence of the total energy is obtained by proper scaling of the individual positions $\mathbf{r}_{\rm N}$ with $a \sim \rho^{-1/3}$ while the individual momenta are scaled with $\rho^{1/3}$.

A snapshot of the quark density (for fixed z) at normal nuclear matter density ρ_0 is shown in the upper part of Fig. 4; the resulting effective mass $m_{\rm u}(\mathbf{r})$

according to the gap equation (8) - for the configuration shown in the upper part of Fig. 4 - is displayed in its lower part. Since at normal nuclear matter density the overlap of the nucleons is only moderate, the individual scalar 'quark bags' can still approximately be separated in space for a given time. As a consequence the average quark mass follows according to the Hellmann-Feynman theorem and the GOR relation (7) [47]

$$m^*(\rho_0) = m_V^*(1 - \frac{\Sigma_{\pi N}}{f_\pi^2 m_\pi^2}\rho_0) \approx 0.65\ m_V^*\ , \tag{17}$$

where m_V^* is the vacuum effective mass from (6).

A further problem is related with the change of the nucleon formfactor in the medium. As suggested e.g. by the interpretation of the EMC effect in ref. [48] or arguments based on chiral symmetry by Brown [16] the nucleon might change its size in the nuclear medium such that the vector density of a quark is no longer given by (9). We account for such in-medium effects by modifying the width parameter b_0 in (9) as

$$b_0(\rho_{\rm N}) = 0.25\,{\rm fm}\left(1 + \alpha\ \frac{\rho_{\rm N}}{\rho_0}\right) \tag{18}$$

with a parameter α to be determined by the nuclear matter saturation point (see below).

As an example we show a snapshot of the quark distribution at $4 \times \rho_0$ for $\alpha = 0.18$ in Fig. 5 (upper part) together with the corresponding quark mass $m^*(x, y, z =\text{const})$ (lower part) from the gap equation (8). Since the overlap of the quark distributions now becomes substantial, the average quark mass drops to about 30 MeV indicating partial chiral symmetry restoration.

As is well known from elastic proton-nucleus scattering [49] the scalar nucleon selfenergy shows an explicit momentum dependence which is not accounted for in the traditional mean-field theory of Walecka [24]. Consequently one also has to investigate the question of the momentum dependence of the effective quark mass. In this respect we turn back to the quark phase-space configuration depicted in Fig. 2 and show in Fig. 6 the resulting effective mass $m^*(\rho_{\rm q}, P)$ for $P_1 = P_2 = P, \rho^1 = \rho^2 = \rho_{\rm q}$ to illustrate the smooth general dependence on density and relative momentum. It is clearly seen from Fig. 6 that the effective mass drops with density ρ and increases for fixed ρ with the relative momentum $P_{\rm r} = 2P$ thus leading to a reduced scalar attraction for higher relative momentum.

Technically the nonlinear solutions for $m_{\rm u}$ and $\rho_{\rm S}$ are stored on a grid as a function of P_1, P_2, ρ^1, ρ^2 and serve as input for the futher computations.

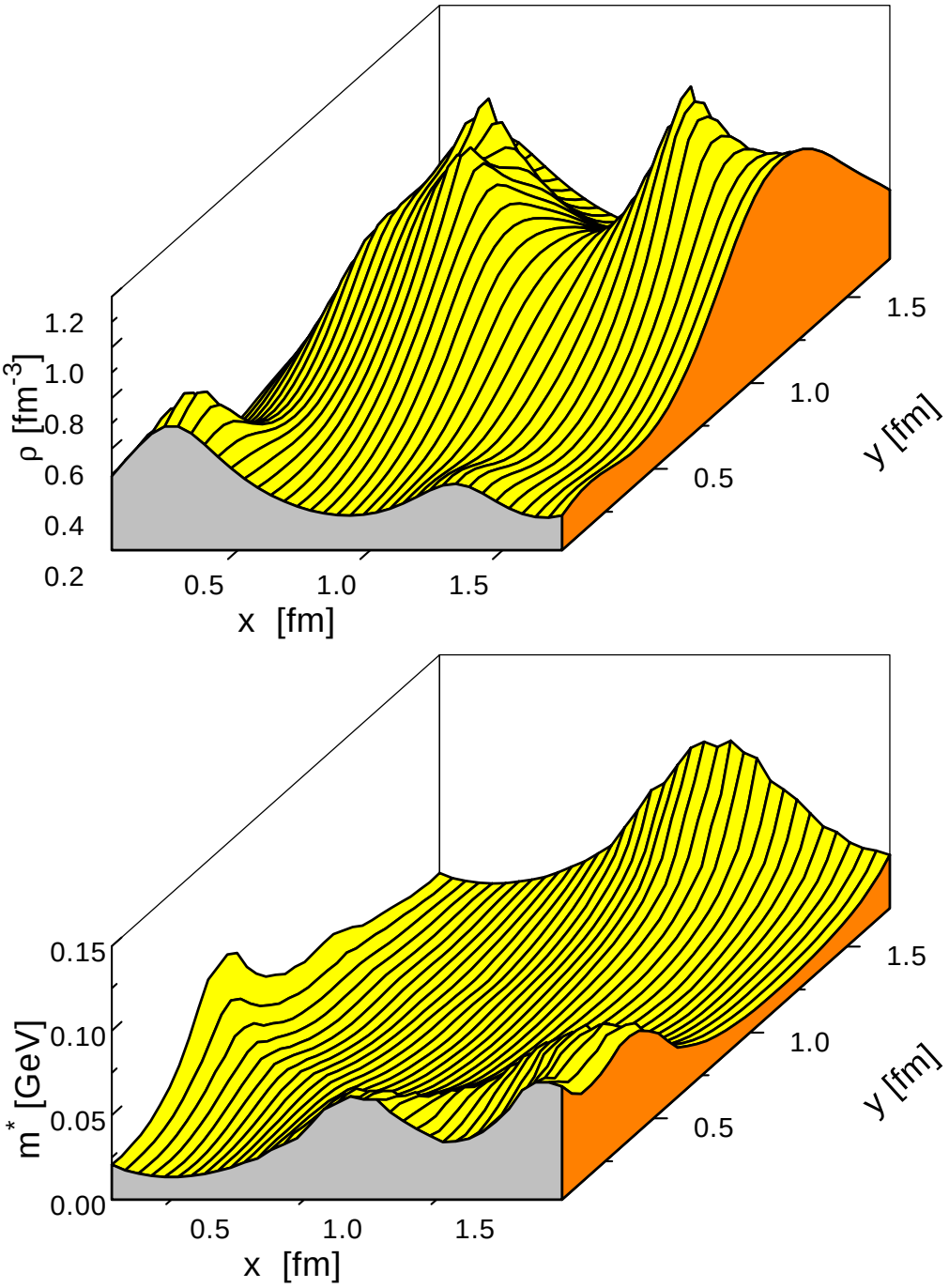

Fig. 4. Snapshot of the spatial quark distribution (for fixed z) at normal nuclear matter density ρ_0 (upper part) together with the resulting effective quark mass m^* (lower part).

Whereas the momentum dependence of the scalar sector now is fixed by the gap equation (8), we have to deal furtheron with slight modifications of the Lorentz vector interaction which for nucleons is known to show an explicit momentum dependence, too [49]. Corresponding nonlocal generalizations of

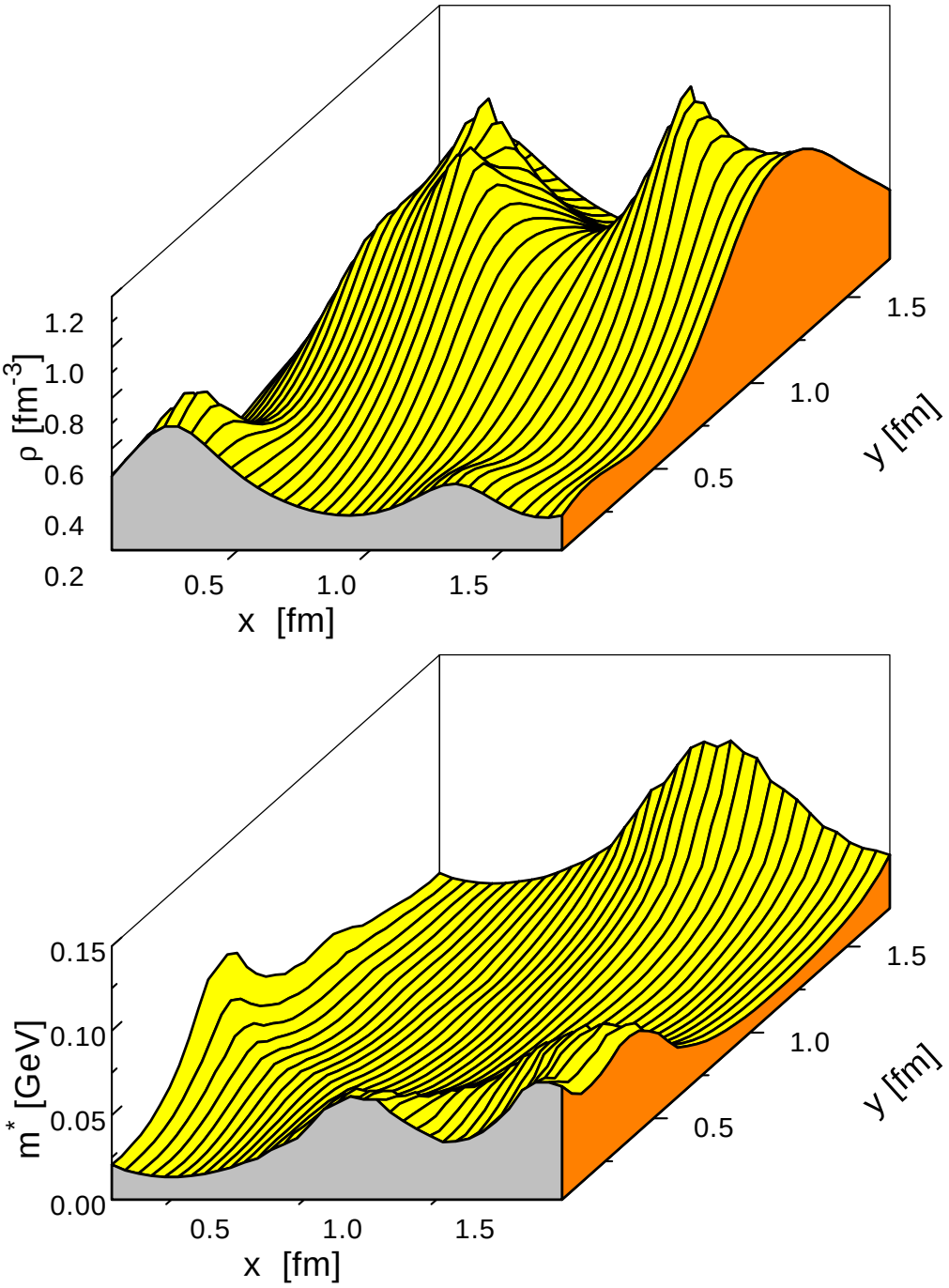

Fig. 5. Snapshot of the spatial quark distribution (for fixed z) at $4 \times \rho_0$ (upper part) together with the resulting effective quark mass m^* (lower part).

the NJL Lagrangian have been suggested by Bowler and Birse [50]. We thus adopt a similar concept and assume that the vector interaction in (13) is

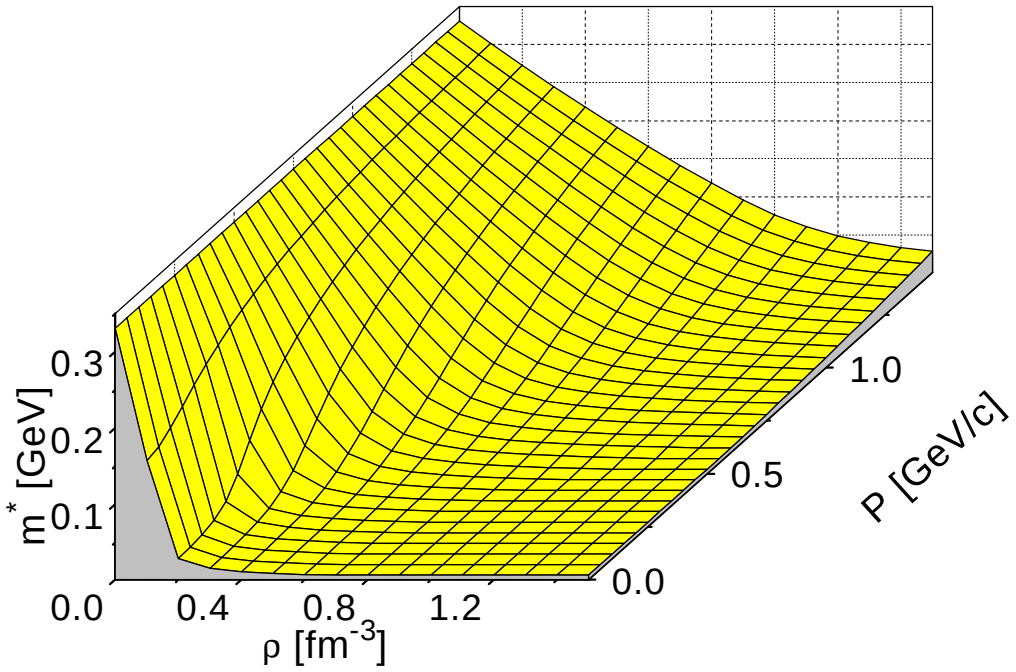

Fig. 6. Effective quark mass m^* as a function of $P = P_1 = P_2$ and $\rho_q = \rho^1 = \rho^2$.

mediated by massive color neutral gluons which implies to modify the coupling

$$G_V \to G_V \frac{\Lambda_V^2}{\Lambda_V^2 + \mathbf{q}^2} \tag{19}$$

where $\Lambda_V \approx 1.2 - 1.5$ GeV either stands for the glue ball mass or simply a vector cutoff, respectively, and $\mathbf{q}$ denotes the momentum transfer in the quark-quark interaction. This strategy is similar to that used in effective meson-exchange interactions for hadron-hadron scattering [51]. Fixing $\Lambda_V \approx 1.5$ GeV the energy density for almost arbitrary nucleon configurations $f_N(\mathbf{r}_N, \mathbf{p}_N)$ then is given by eq. (13) and the total energy of the configuration is obtained by integration over $\int d^3r\ T^{00}(\mathbf{r})$.

Before evaluating the energy density for nuclear matter configurations we have to make sure that for vanishing nuclear density the energy of a nucleon moving with momentum $p_N = 3p_q$ agrees with the dispersion relation of a free nucleon, i.e.

$$E(p_N) = \sqrt{p_N^2 + M_N^2}\ , \tag{20}$$

where M_N is the nucleon mass in its rest frame. This is indeed the case as shown in Fig. 7, where the relation (20) (solid line) is compared to the result from integrating $T^{00}(\mathbf{r})$ over $\mathbf{r}$ (dotted line). The slight deviations from the

exact result (20) provide a measure of the numerical accuracy achieved in the computations.

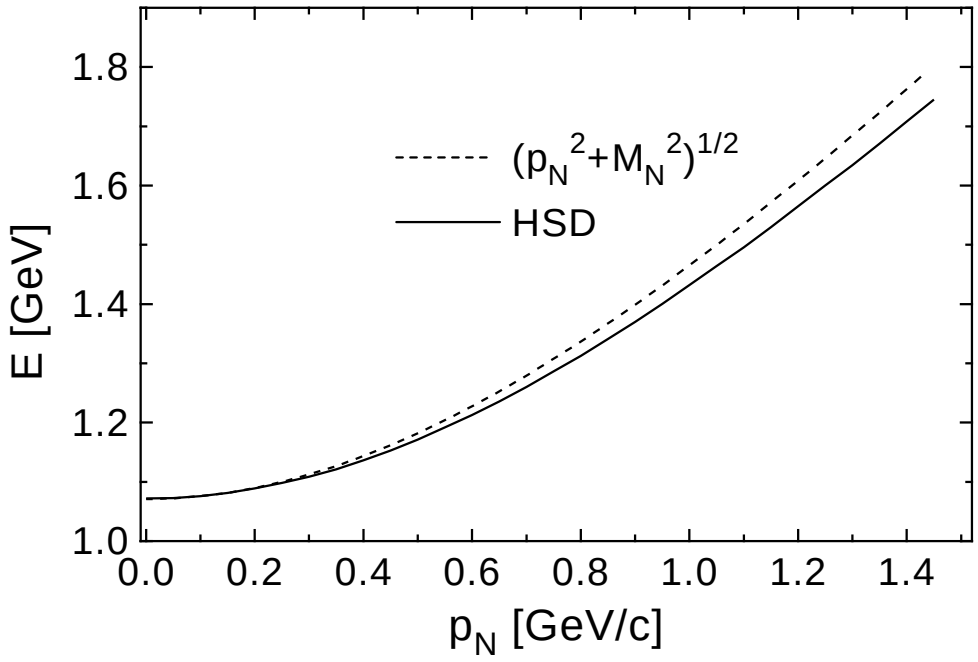

Fig. 7. Free nucleon dispersion relation (20) (solid line) and $\int d^3r\ T^{00}(\mathbf{r})$ (dotted line) for a 'nucleon' moving with momentum $P_{\rm N}$.

Now performing the integration of T^{00} over coordinate space and averaging over characteristic samples for nuclear matter configurations (as shown in Fig. 4) [2], dividing by the number of nucleons on the grid and subtracting the bare nucleon mass we can compute the energy per nucleon $E/A(\rho/\rho_0)$ and thus establish a direct link between the energy density of quarks with the energy per nucleon of isospin symmetric nuclear matter at finite nucleon density ρ/ρ_0. The resulting energy per nucleon (nucleon mass subtracted) (for $\alpha = 0.18$) is shown in Fig. 8 (full line) [3] in comparison to the Dirac-Brueckner results from [13] (full squares) and the parametrizations POL6 and POL7 of the RBUU approach [7] that were found to optimally describe heavy-ion reactions in the energy regime up to about 1 GeV/A [9]. We find the binding energy per nucleon (≈ -16 MeV at $\rho_{\rm N} = \rho_0$) to be reproduced well for $\alpha \approx 0.18$ which

[2] For technical reasons we first look for the 'nucleon' that exhibits a maximum quark density at a given grid point $\mathbf{r}$ (giving ρ^1, P_1) and then sum up the quark contributions of the other 'nucleons' (giving ρ^2, P_2). The corresponding values for m^* and $T^{00}(\mathbf{r})$ are the taken from the parametrized configurations displayed in Fig. 2. We have tested for a couple of samples that this approximate evaluation works quite well if ensemble averages for nuclear matter configurations are considered.

[3] The model described here is denoted by **H**adron-**S**tring-**D**ynamics (HSD) (see below).

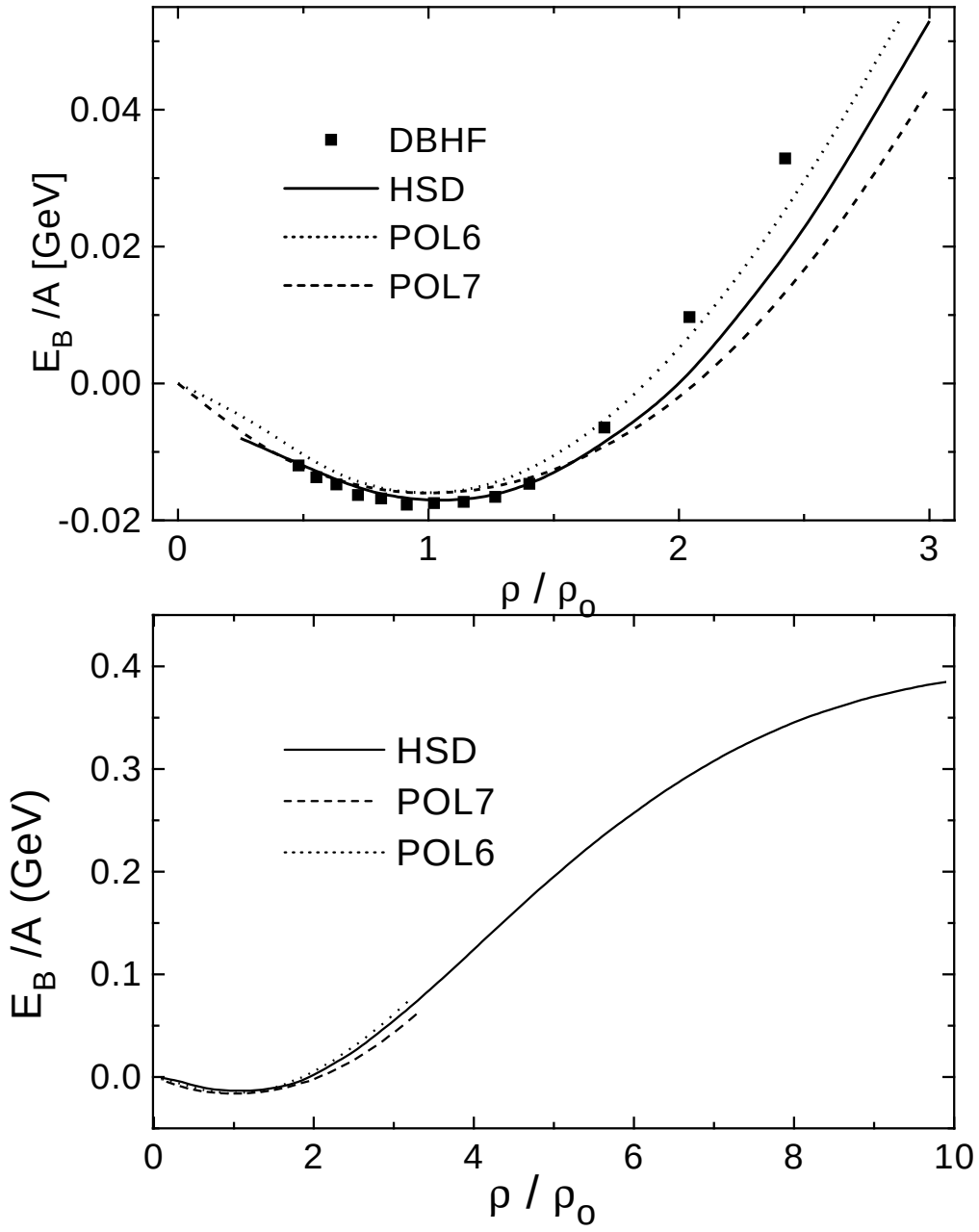

Fig. 8. Equation of state for nuclear matter; HSD (solid line), DBHF (full squares); RBUU results: POL6 (dotted line), POL7 (dashed line) from ref. [9].

corresponds to a swelling of the nucleon by 18% at normal nuclear matter density. For $\alpha = 0$ there is no minimum in the energy per nucleon due to the Pauli pressure such that the swelling of the nucleon - which enhances the scalar attraction and reduces the vector repulsion - is a necessary phenomenon within the present approach to achieve proper binding. We note that the resulting incompressibility K of nuclear matter amounts to about $K \approx 250$ MeV. Since the energy per nucleon in our approach (HSD) is well in between the limits of

POL6 and POL7 as extracted from detailed comparisons in ref. [9] for nucleus-nucleus collisions in the SIS energy regime, we infer that the equation of state generated by the model is quite realistic in the lower density ($\rho \leq 3\rho_0$) regime. Its extension to $10\rho_0$ (lower part of Fig. 8), however, is questionable and has to be examined in comparison to experimental flow data at much higher (e.g. AGS) bombarding energies.

Via the simulation of nuclear matter configurations - as described above - we are now in the situation to establish a close connection between scalar and vector quark densities and scalar and vector nucleon densities. The key link in this respect is given by relation (17) at low nucleon density. In this respect we show in Fig. 9 the average effective quark mass (in units of the vacuum mass m_V^*) (solid line) as a function of the nuclear density ρ_N as obtained from the nuclear matter simulations. As discussed before, the effective quark mass drops by about 35 % at ρ_0 according to (17), however, essentially continues with a constant slope up to about $2 \times \rho_0 \approx 0.33\text{fm}^{-3}$ in line with the Dirac-Brueckner analysis in ref. [52](cf. also ref. [53]). The bare quark mass then is reached at about $\rho \approx 0.6\text{fm}^{-3}$. It is worth noting that the effective nucleon mass (normalized to the vacuum mass) in the RBUU approach of ref. [9] shows the same scaling with density up to about ρ_0 which is also well in line with Dirac phenomenology. As a consequence it is natural to define a nucleon scalar

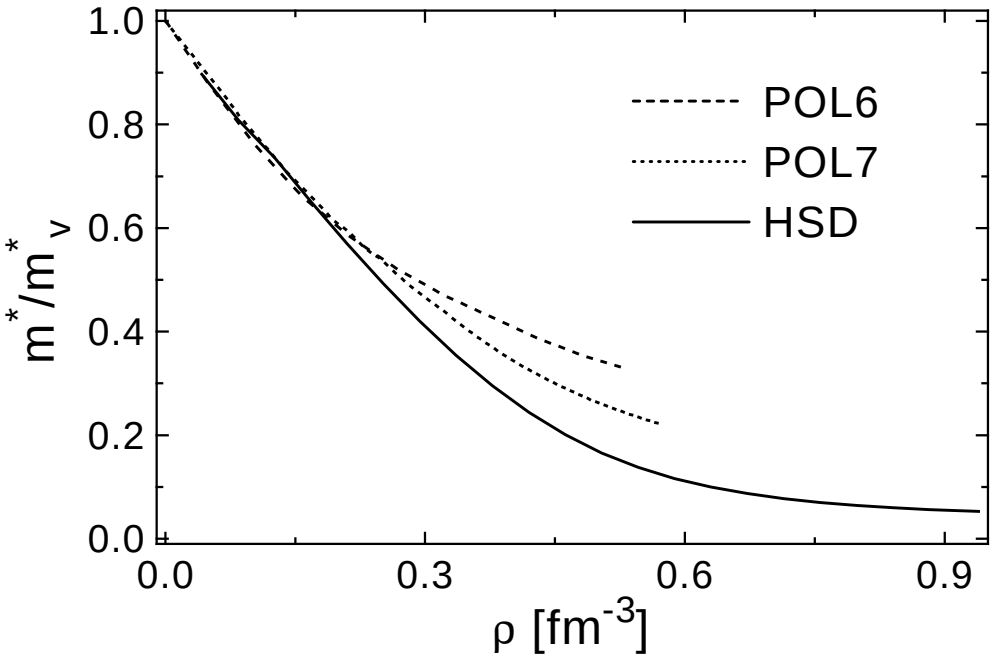

Fig. 9. Effective mass divided by the vacuum mass; quark mass $m^*(\rho_N)$ in the HSD approach (solid line); nucleon mass in the RBUU approach: POL6 (dotted line), POL7 (dashed line).

selfenergy $U_{\rm S}(\rho)$ in the nuclear medium via the effective quark masses as

$$U_{\rm S}(\rho_{\rm N}) = -M_{\rm N}\ (1 - \frac{m^*(\rho_{\rm N})}{m_V^*}), \tag{21}$$

where $M_{\rm N}$ denotes the free nucleon mass. By eq. (21) the nucleon effective mass $M_{\rm N}^*$ or scalar selfenergy $U_{\rm S}$ is entirely determined by the average quark effective mass m^* generated by the gap equation (8). The nucleon vector selfenergy $U_\mu(\rho_N, p)$ then can be determined from (21) and the numerical result for the EOS in Fig. 8 (solid line) by identifying

$$E/A = T_{\rm N}^{00}/\rho_{\rm N} - M_{\rm N} \tag{22}$$

with the 'nucleon' energy density (cf. ref. [7])

$$\begin{aligned} T_{\rm N}^{00} = & \frac{4}{(2\pi)^3)} \int d^3p \sqrt{p^2 + M_{\rm N}^{*2}} + \frac{1}{2}\rho_S^{\rm N} U_{\rm S} \\ & + \frac{1}{2}\tilde{G}_{\rm V}^2 4^2 \int \frac{d^3p_1}{(2\pi)^3}\frac{d^3p_2}{(2\pi)^3} f_N(p_1) \frac{\Lambda_{\rm V}^2}{\Lambda_{\rm V}^2 + (\mathbf{p}_1 - \mathbf{p}_2)^2} f_N(p_2) \end{aligned} \tag{23}$$

with

$$\rho_{\rm S}^{\rm N} = \frac{4}{(2\pi)^3} \int d^3p \frac{M_N^*}{\sqrt{p^2 + M_N^{*2}}} f_N(p) \tag{24}$$

where now only the nucleon vector selfenergy is still undetermined. Assuming, however, that the momentum dependence of $U_\mu(\rho_{\rm N}, p)$ is the same as for the quarks given by (19) the EOS in Fig. 8 fixes completely also the nucleon vector coupling $\tilde{G}_{\rm V}^2$ and thus the zeroth component of the vector selfenergy U_0 as a function of the nuclear density $\rho_{\rm N}$ i.e.

$$U_0(p) = 4\ \tilde{G}_{\rm V}^2 \int \frac{d^3p'}{(2\pi)^3} \frac{\Lambda_{\rm V}}{\Lambda_{\rm V}^2 + (p - p')^2} f(p') \tag{25}$$

In Fig. 10 we compare the explicit momentum dependence of the nucleon selfenergies at density ρ_0 with Dirac-Brueckner results from [13] (full dots). In the lower part of Fig. 10 the real part of the Schroedinger equivalent potential

$$\begin{aligned} U_{\rm SEP} = & U_{\rm S}(\rho_0, P) + U_0(\rho_0, P) + \frac{1}{2M}(U_{\rm S}(\rho_0, P)^2 - U_0(\rho_0, P)^2) \\ & + U_0(\rho_0, P)\frac{\sqrt{P^2 + M^2} - M}{M} \end{aligned} \tag{26}$$

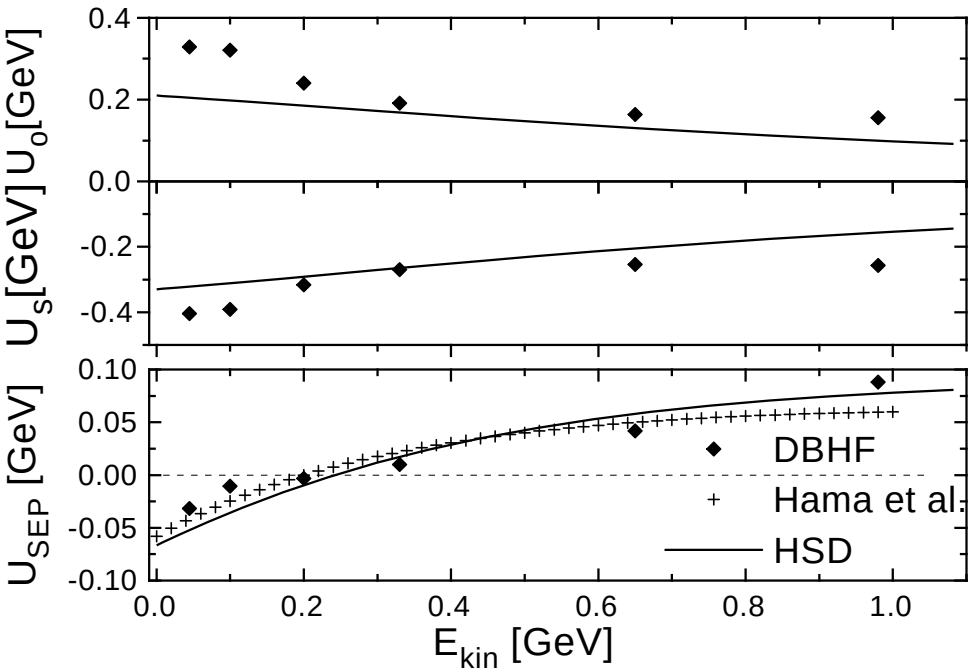

Fig. 10. Nucleon selfenergies $U_{\rm S}$, U_0 and the Schroedinger equivalent potential $U_{\rm SEP}$ as a function of the nucleon kinetic energy $E_{\rm kin}$ with respect to the nuclear matter rest frame. HSD (solid line), DBHF (full squares), exp. data from Hama et al. [49] (crosses).

is additionally shown (full line) in comparison to the optical potential analysis from Hama et al. [49] (dashed line) and Dirac-Brueckner computations from [13] up to momenta of 1 GeV/c. This comparison shows that the overall properties of the nucleon selfenergies are reasonably met by our approach.

Apart from the close analogy of our results with the σ-ω model at 'low' momenta (cf. Fig. 10) we are especially interested in the 'high' momentum properties of the present approach where the standard σ-ω model is known to fail significantly. This deficiency has been especially addressed in the works by Weber et al. [7–9] where an explicit momentum dependence has been introduced by Fock diagrams of similar form as (25); however, the extrapolation of this ansatz to momenta of a few GeV/c is quite uncertain. The respective results from our present approach for the scalar and vector nucleon selfenergy as well as the Schroedinger equivalent optical potential in analogy to Fig. 10 are displayed in Fig. 11 up to relative kinetic energies of 15 GeV. Whereas the scalar and vector nucleon selfenergies are found to gradually decrease with momentum (or kinetic energy) - which is a direct consequence of the cutoff $\Lambda_v \approx 1.5$ GeV or scalar glueball mass introduced in eq. (19) - the Schroedinger equivalent potential exhibits a maximum of about 60 MeV at 1 GeV and drops again for higher momenta. Thus we expect the effects from the real part of the nucleon selfenergies to be of minor importance in

the initial phase of nucleus-nucleus collisions at bombarding energies of a few GeV/A, where nucleon cascading with inelastic nucleon excitations should be dominant, i.e. the imaginary part of the hadron selfenergies.

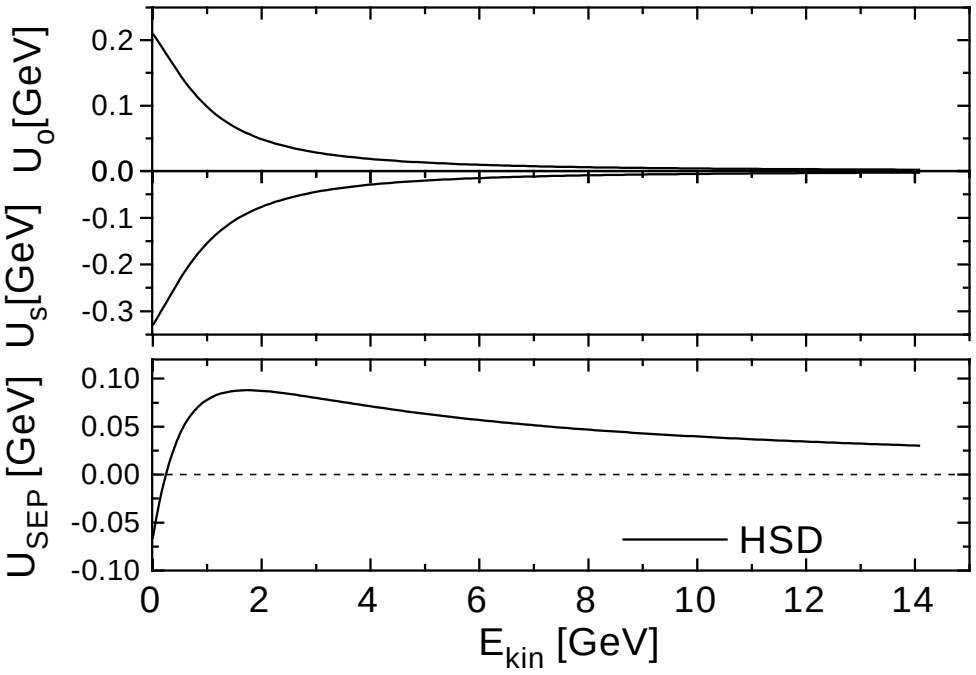

Fig. 11. Nucleon selfenergies $U_{\rm S}$, U_0 and the Schroedinger equivalent potential $U_{\rm SEP}$ as a function of the nucleon kinetic energy $E_{\rm kin}$ at normal nuclear matter density ρ_0.

4 Elastic and inelastic hadron scattering

Whereas in a fully selfconsistent relativistic transport theory the real part and the imaginary part of hadron selfenergies are related by means of dispersion relations [1,3,13], it is not justified to employ the model selfenergies (determined in Section 3) in dispersion integrals for the imaginary part because the inelastic scattering rate of nucleons and mesons turns out to be wrong in the limit of vanishing baryon density. We thus write the coupled set of transport equations for the hadron phase-space distributions $f_{\rm h}(x,p)$ in the more familiar form with interaction rates [1] instead of the imaginary part of the hadron selfenergy

$$\left\{\left(\Pi_\mu - \Pi_\nu \partial^p_\mu U^\nu_{\rm h}\right)\partial^\mu_x - M^*_{\rm h}\partial^p_\mu U^{\rm S}_{\rm h}\partial^\mu_x + \Pi_\nu\left(\partial^x_\mu U^\nu_{\rm h} + M^*_{\rm h}\partial^x_\mu U^{\rm S}_{\rm h}\right)\partial^\mu_p\right\} f_{\rm h}(x,p)$$
$$= \sum_{\rm h_2 h_3 h_4 \ldots} \int d2d3d4\ldots [G^\dagger G]_{12\to 34\ldots}\delta^4_\Gamma(\Pi + \Pi_2 - \Pi_3 - \Pi_4\ldots)$$

$$\times \Big\{ f_{\rm h_3}(x,p_3) f_{\rm h_4}(x,p_4) \bar{f}_{\rm h}(x,p) \bar{f}_{\rm h_2}(x,p_2)$$
$$- f_{\rm h}(x,p) f_{\rm h_2}(x,p_2) \bar{f}_{\rm h_3}(x,p_3) \bar{f}_{\rm h_4}(x,p_4) \Big\} \ldots \qquad (27)$$

In eq. (27) $U_{\rm h}^{\rm S}$ and $U_{\rm h}^{\mu}$ denote the real part of the scalar and vector hadron selfenergies, respectively, while $[G^+G]_{12\to 34\ldots}\delta_\Gamma^4(\Pi + \Pi_2 - \Pi_3 - \Pi_4 \ldots)$ is the transition rate for the process $1+2 \to 3+4+\ldots$ which is taken to be on-shell in the semiclassical limit adopted [4]. The quasi-particle properties are defined via the mass-shell constraint [7],

$$\delta(\Pi_\mu \Pi^\mu - M_{\rm h}^{*2}), \qquad (28)$$

with effective masses and momenta given by

$$M_{\rm h}^*(x,p) = M_{\rm h} + U_{\rm h}^{\rm S}$$
$$\Pi^\mu(x,p) = p^\mu - U_{\rm h}^\mu(x,p). \qquad (29)$$

The phase-space factors

$$\bar{f}_{\rm h}(x,p) = 1 \pm f_{\rm h}(x,p) \qquad (30)$$

are responsible for fermion Pauli-blocking or Bose enhancement, respectively, depending on the type of hadron in the final/initial channel. Explicitly propagated in the following are nucleons, Δ's, N(1440), N(1535), Λ and Σ hyperons for the baryons and pions, kaons, η's, K*'s, ρ's, ω's and Φ's as mesons together with their respective antiparticles. As a first approximation we assume that all baryons (made out of light (u,d) quarks) have the same scalar selfenergies as the nucleons (cf. Section 3); the vector selfenergy for antiparticles is introduced with a relative (-) sign according to time reversal[5] while the hyperons pick up a factor 2/3 according to the light quark content.

For the inelastic channels we restrict to binary hadron-hadron collisions. As known from transport studies at energies below 2 GeV/A the elementary cross sections in eq. (27) may be approximated by their values in free space. Thus as a first step we adopt the same strategy and use the explicite cross-sections as in the BUU model [54] (for $\sqrt{s} \leq 2.6$ GeV) - that have been successful tested in the energy regime below 2 GeV/A bombarding energy - and by the LUND string formation and fragmentation model [41] (for $\sqrt{s} > 2.6$ GeV) in case of

[4] The index Γ at the δ-function indicates that off-shell transitions of width Γ should also be allowed. In the actual transport simulation, however, we use the on-shell limit $\Gamma = 0$.

[5] This limit has to be taken with care because Teis et al. found in [3] that a sign change of the vector potential results in a too strong attraction for antiprotons.

baryon-baryon collisions. For meson baryon reactions we adopt a transition energy of $\sqrt{s} = 1.8$ GeV between the known low energy cross sections and the LUND model. We note that the actual values for the transition energies in the elementary cross sections are not sensitive to nucleus-nucleus collisions in the energy regime to be discussed in Section 5.

In order to obtain a rough idea about the inelastic cross sections from the LUND string fragmentation model, we show in Fig. 12 the rapidity spectra for baryons, pions, kaons, ρ and ω mesons from pp collisions at $T_{\rm lab} = 20$ GeV in the pp center-of-mass system. Whereas the baryons turn out to be located in rapidity close to the initial rapidity of the two colliding baryons, the meson rapidities are dominantly centered around midrapidity with a small contribution from the deexcitation of the baryonic constituents close to the incoming baryon rapidities. This general tendency has to be kept in mind when comparing to nucleus-nucleus collisions later on.

The implementation of the LUND string formation and fragmentation model [41] - which describes the free transition probabilities - in a covariant transport theory implies to use a time scale to transform the cross-sections to collision rates and particle production rates. An appropriate time scale is given by a string formation time $\tau_{\rm for}$ which denotes the time between the formation and fragmentation of the string in the individual hadron-hadron center-of-mass system for a particle of rapidity $y_{\rm cm} = 0$. Due to covariance this time should be also related to the spatial extension of the interacting hadrons which on average gives $\tau_{\rm for} \approx 0.8$ fm/c. Changing this formation time by $\pm$ 20% does not substantially alter the results to be presented in Section 5; we note, that similar values are also adopted in the RQMD approach [55].

In view of the 'chiral dynamics' addressed in this work, however, especially the productions rates of mesons should change at high baryon density [56] due to the reduced masses involved. Unfortunately, the actual meson scalar and vector selfenergies are quite a matter of debate and depend on the model parameters of the Lagrangians employed. Whereas the Lagrangian (2) does not provide a coupling between u,d and s quarks on the mean-field level, alternative models [57] do include such couplings. The average mass of a K^+ K^- pair e.g. according to ref. [57] is expected to follow

$$m^*_{\rm K^+K^-} \approx m^*_{\rm V}(1 - 0.16\rho_{\rm N}/\rho_0). \tag{31}$$

Independently, also QCD sum rules provide a scaling of mesons in the medium, e.g. Hatsuda and Lee obtain for ρ and Φ mesons [58]

$$m^*(\rho_{\rm N}) \approx m_{\rm V}(1 - \lambda\rho_{\rm N}/\rho_0) \tag{32}$$

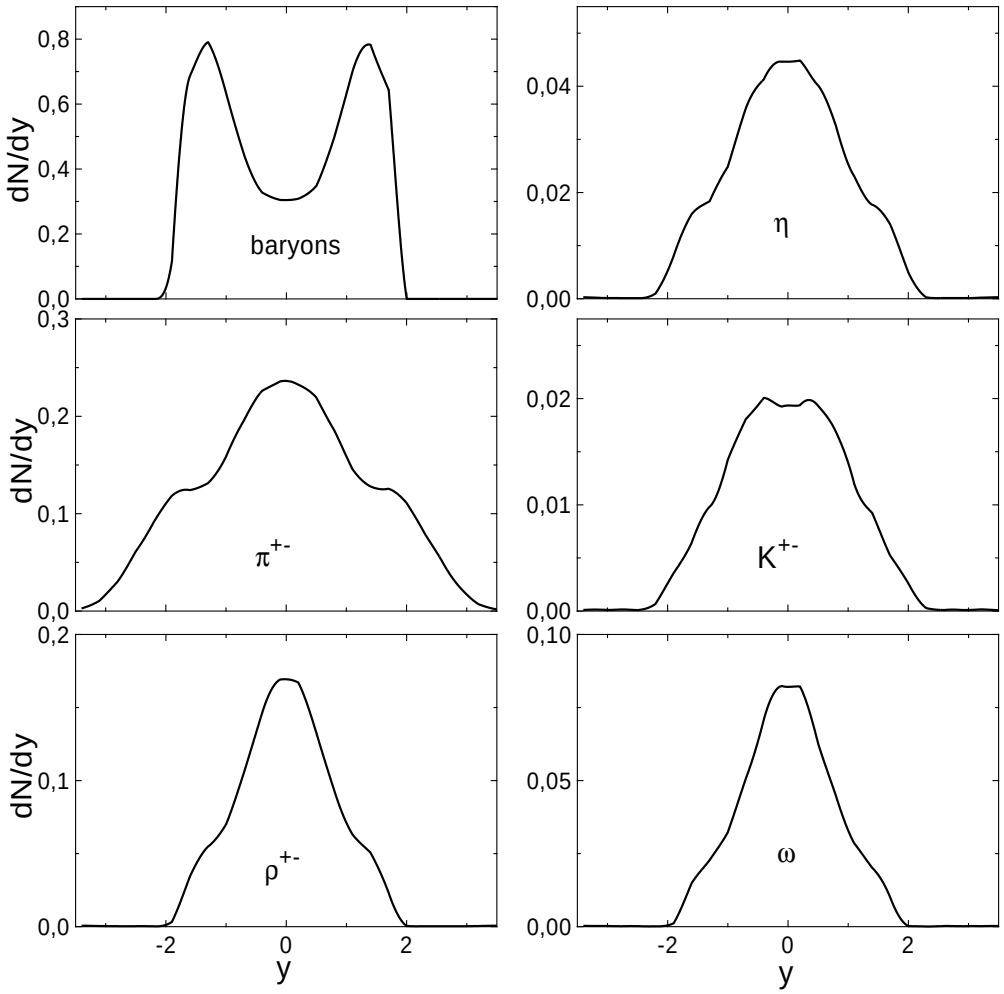

Fig. 12. Rapidity distributions for baryons, pions, kaons, η, ω and ρ mesons from the LUND string fragmentation model for pp collisions at $T_{\rm lab}$ = 20 GeV.

with $\lambda \approx 0.18$ for ρ and ≈ 0.025 for Φ mesons. The weak dependence of the Φ meson mass here is a consequence of the weak coupling of the strange quark to the light (u,d) quarks which dominantly make up the baryon density.

In view of the substantial uncertainties of the meson selfenergies especially at high density we here propose a *pragmatic model* which does not claim fundamental evidence[6]. Whereas the pion as a Goldstone boson is assumed not to change substantially with baryon density and temperature in the energy regime addressed, the kaons, η's, K*'s, ρ's, ω's and ϕ's are assumed to change their masses as displayed in Fig. 13 roughly in line with ref. [57,58] as pointed out above. The final values achieved at high baryon density are determined by the bare quark mass content of the mesons.

[6] These assumptions about meson properties at high baryon density can only be controlled in confrontation with sensitive experimental data.

The relativistic coupled channel transport approach described above will be denoted by **H**adron-**S**tring-**D**ynamics (**HSD**) furtheron.

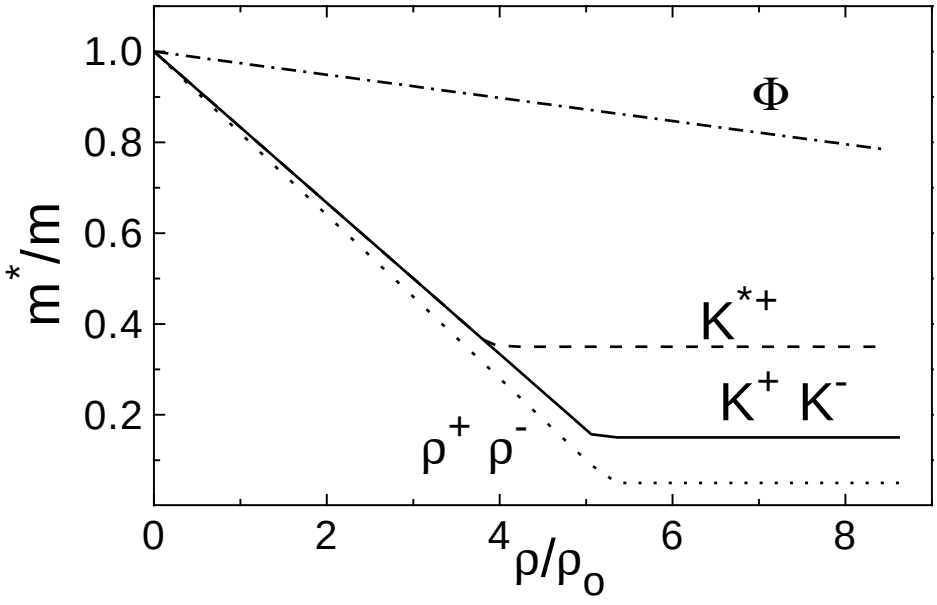

Fig. 13. Parametrization of the effective meson masses versus the baryon density used in the extended string fragmentation model (HSD).

As an example for the effects to be expected at high baryon density we show in Fig. 14 the rapidity spectra of kaons and ρ's for pp collisions at $T_{\rm lab}$ =20 GeV from the string fragmentation model that incorporates the density dependent meson masses from Fig. 13. It is clearly seen that a dropping of the meson masses leads to a substantial enhancement of the K^+K^- and ρ yields and to a widening of their rapidity distribution in the individual center-of-mass system. If such phenomena can be seen in comparison to experimental data will be investigated in the next Section.

5 Heavy-ion-collisions

The relativistic transport approach (HSD) outlined above now is applied to nucleus-nucleus collisions from the SIS to the SPS energy regime with particular emphasis on rapidity distributions and particle spectra to control the stopping achieved in these reactions. The explicit numerical implementation of the selfenergies and collisions rates is performed in close analogy to [9,54,59,60] and does not have to be repeated here. We note that the total conservation of energy and momentum throughout the time evolution is conserved on the 2

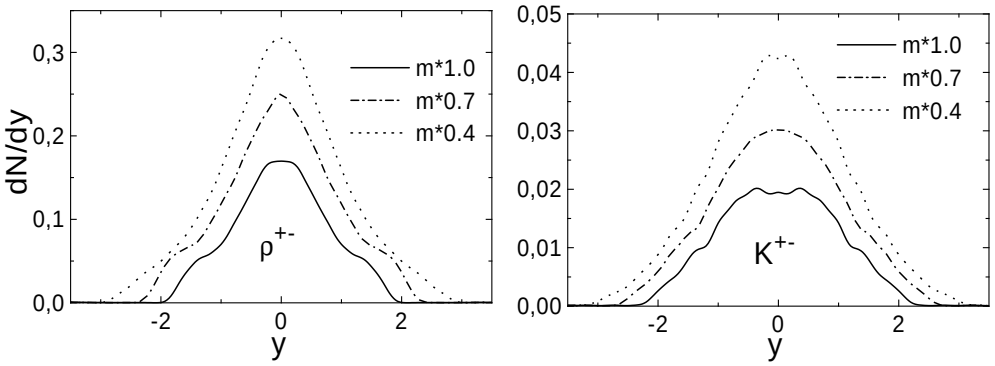

Fig. 14. Differential $K^+ + K^-$ and ρ rapidity distributions from the 'chiral' string fragmentation model at 1.0, 0.7 and 0.4 $\times$ the bare masses for pp collisions at $T_{\rm lab}$=20 GeV.

% level for central Au + Au collisions and even better for peripheral or light ion induced reactions.

As a first example we show in Fig. 15 the transverse π^0-spectra from Ar + Ca collisions at 1.5 GeV/A in comparison to the data of [61] as a characteristic system at SIS energies. Since at these energies the present approach is close to the results achieved with the former BUU model [62], the reproduction of the data is of similar quality. We thus conclude that the 'low energy dynamics' involving essentially nucleons, Δ's and pions is reasonably well included in our transport calculations.

5.1 Stopping in high-energy nucleus-nucleus collisions

The next system addressed is Si + Al at 14.6 GeV/A, i.e. the AGS energy regime. The computed rapidity distribution of protons and π^+-mesons for b = 1.5 fm is compared in Fig. 16 to the data from ref. [63]. Whereas the proton rapidity distribution turns out to be quite flat in rapidity y due to proton rescattering, the pion rapidity distribution is essentially of gaussian shape which reflects the pion rapidity spectrum from the string fragmentation model outlined in Section 4 (cf. Fig. 12). The flat proton rapidity spectrum might lead to the interpretation that there is a substantial amount of stopping in the light system Si + Al. This, however, has to be taken with care because the actual snapshots of the baryon density distribution from our computations shown in Fig. 17 (l.h.s.) as well the phase-space distribution (r.h.s.)

$$f(z,p_z;t) = (2\pi)^{-2} \sum_b \int dr_\perp dp_\perp f_b(r_\perp, z, p_\perp, p_z; t), \tag{33}$$

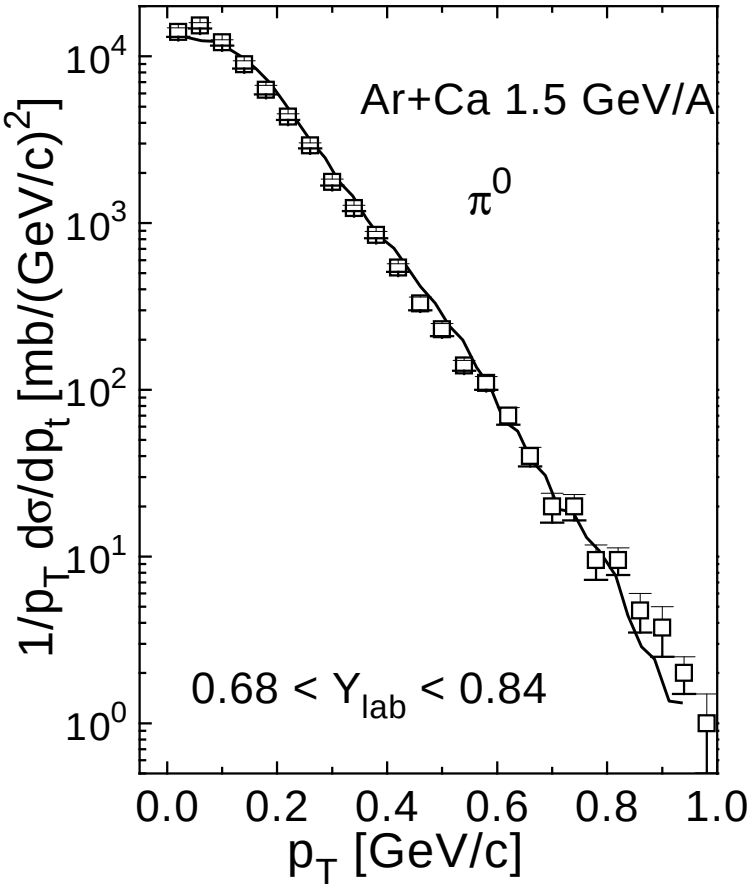

Fig. 15. Calculated transverse π^0-spectra for Ar + Ca at 1.5 GeV/A (full line) in comparison to the experimental data from ref. [61].

where $\sum_b$ denotes a sum over all baryon species, indicate a dominant transparency for the light system. This is essentially due to the large surface of the two light nuclei with a nucleon-nucleon collision probability less than 1.

The amount of stopping at AGS energies is more clearly pronounced for central Au + Au reactions as displayed in Fig. 18 for the proton and π^+ rapidity distributions.

Though the pion rapidity spectrum does not differ very much in shape from that of the Si + Al system in Fig. 16 at first sight, the time evolution of the baryon distribution in coordinate space, momentum space and phase space (Fig. 19) for Au+Au at 14.6 GeV/A shows a clear approach versus equilibration. However, the coordinate space evolution indicates a dominant longitudinal expansion which is also reflected in the baryon momentum distribution that does not show full isotropy. Detailed experimental data and related comparisons, however, will become available soon at the energy of 10.8 GeV/A

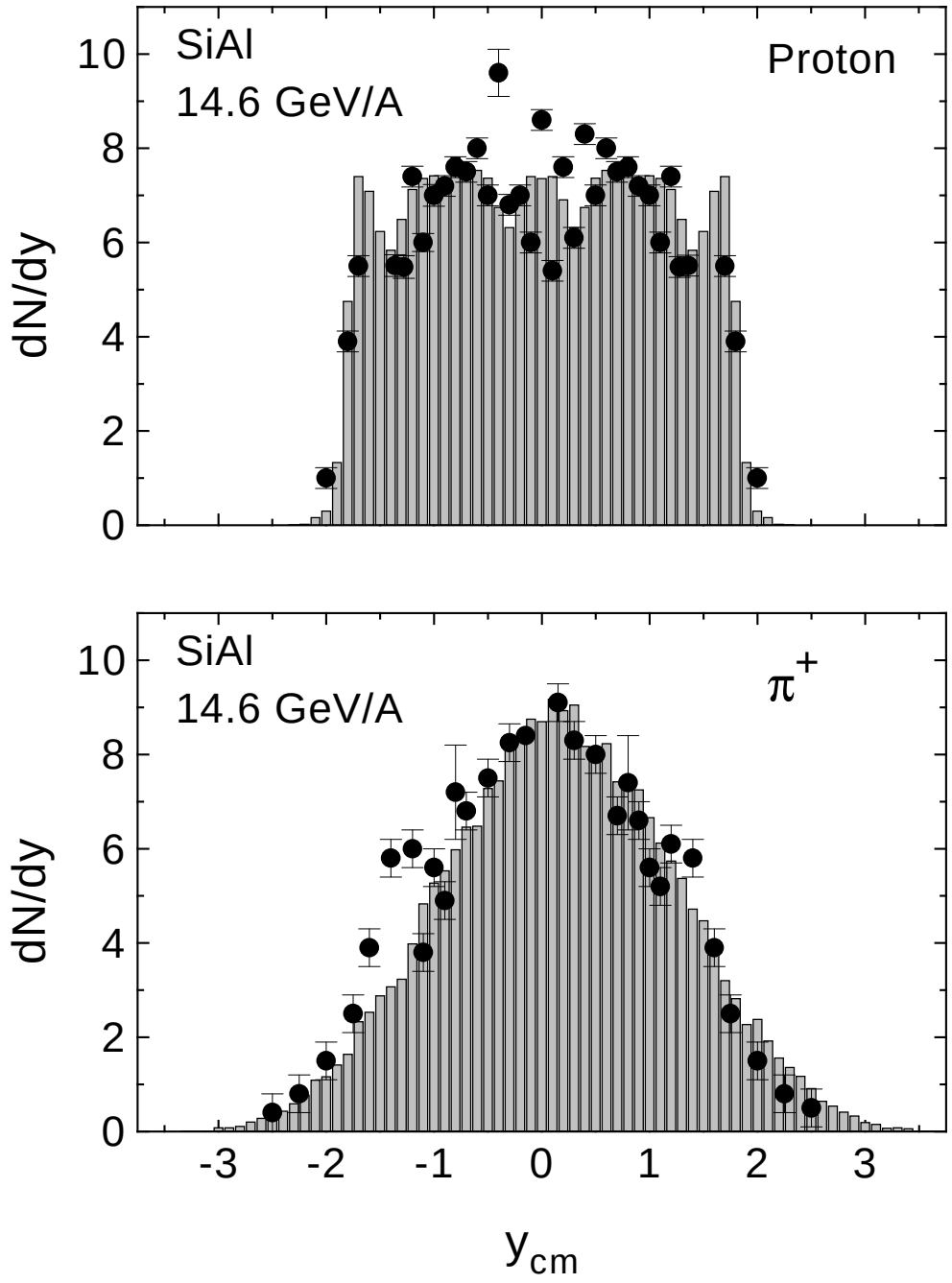

Fig. 16. Calculated proton and π^+ rapidity distribution (histrograms) for a central 14.6 GeV/A Si+Al collision in comparison to the data from [63] (full dots).

[64]. We note that the proton rapidity spectrum for central Au + Au collisions at this energy shows a similar amount of stopping as the RQMD approach [55].

We continue our comparison to experimental data with the system S + S at 200 GeV/A, i.e. the SPS regime (Fig. 20). Though the experimental proton and pion rapidity spectra (from [65]) are approximately reproduced, we cannot

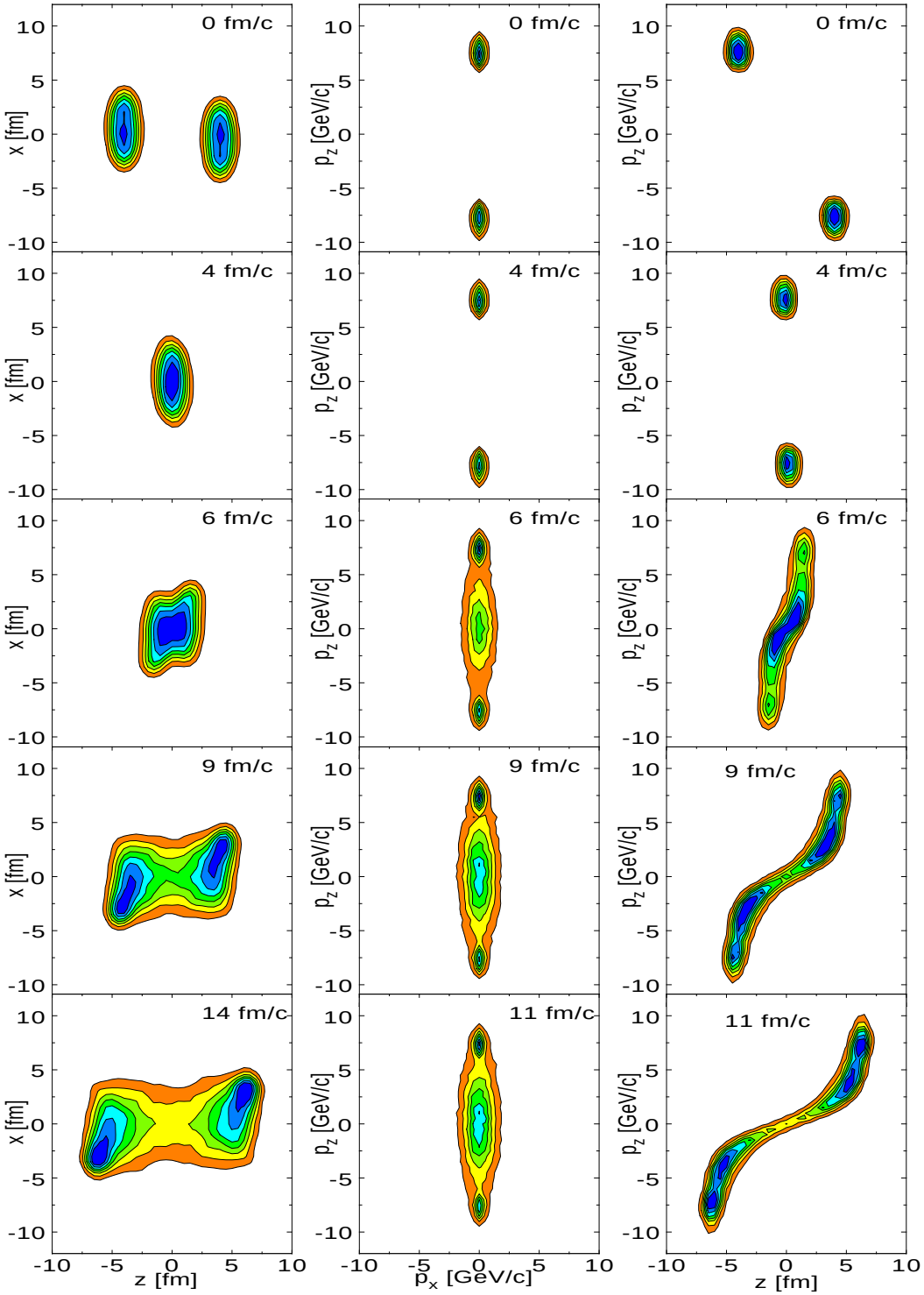

Fig. 17. Baryon density distribution (left column), momentum space (middle column) and phase-space distribution (right column) for a 14.6 GeV/A Si+Al collision at b = 1 fm for various times in fm/c.

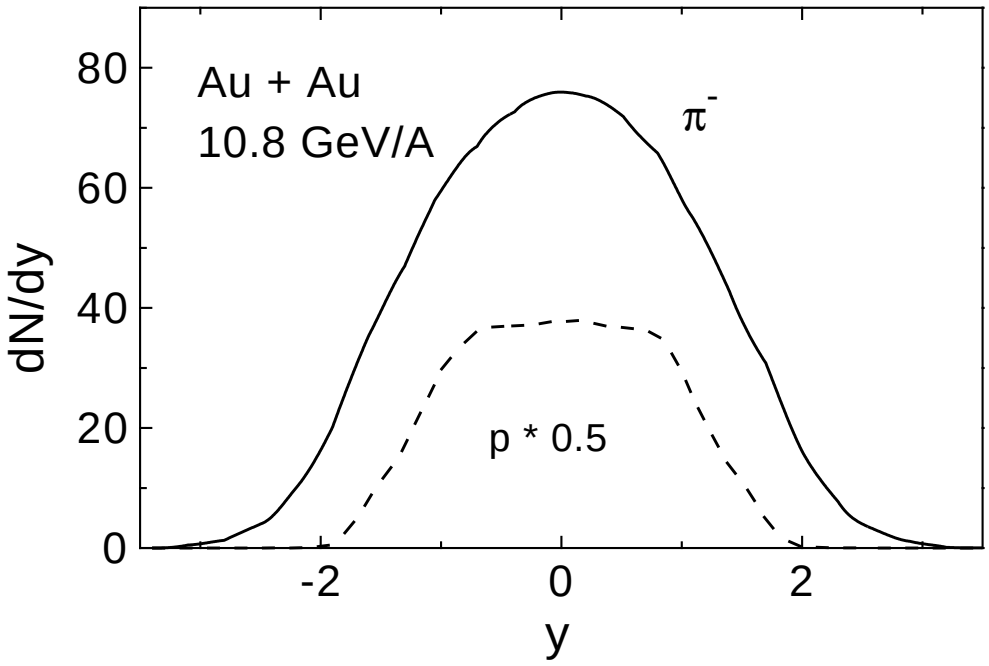

Fig. 18. Proton (dashed line) and π^- rapidity distribution (full line) for a central 10.8 GeV/A Au + Au collision.

conclude on the general applicability of our approach at SPS energies because also more simple models like HIJING or VENUS - with a less amount of rescattering - can reproduce the data in a similar way [66]. A way out of this problem is to analyze the system Pb + Pb at 153 GeV/A (Fig. 21) that has recently been studied experimentally at the SPS. Our computed proton rapidity spectrum for central collisions shows no dip at midrapidity as in HIJING or VENUS simulations [66] but a flat spectrum similar to RQMD simulations [55]. On the other hand, the pion rapidity distributions are very similar to the S + S case, however, enhanced by about a factor of 7.

5.2 Probing chiral symmetry restoration

The problem of chiral symmetry restoration can be addressed e.g. via the K^+/π^+ ratio as addressed in [56]. For this purpose we show in Table 5.2 the calculated K^+/π^+ yields for the systems p + P, Si + Al, Si + Au and Au + Au at 14.6 GeV/A in comparison with the experimental data for two different szenarios. The first column represents the results of a simulation where only the bare masses of the mesons have been considered in the string fragmentation approach (HSD) whereas the second column results from density-dependent mesons masses as described in Section 4. It is clearly seen that for density-dependent K^+ masses the ratio is strongly enhanced for the heavier systems as

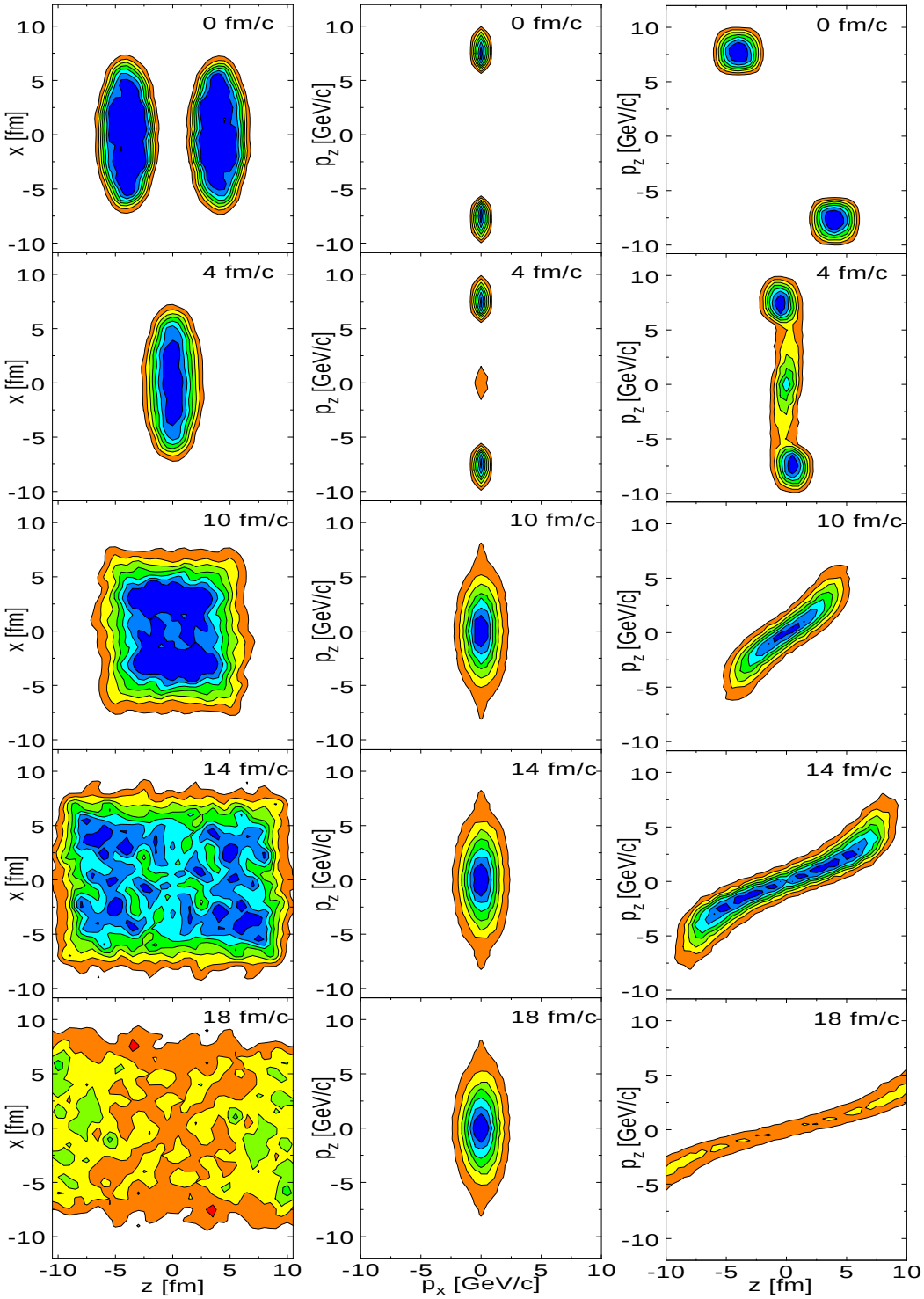

Fig. 19. Baryon density distribution (left column), momentum space (middle column) and phase-space distribution (right column) for a 14.6 GeV/A Au + Au collision at b = 0 fm for various times in fm/c.

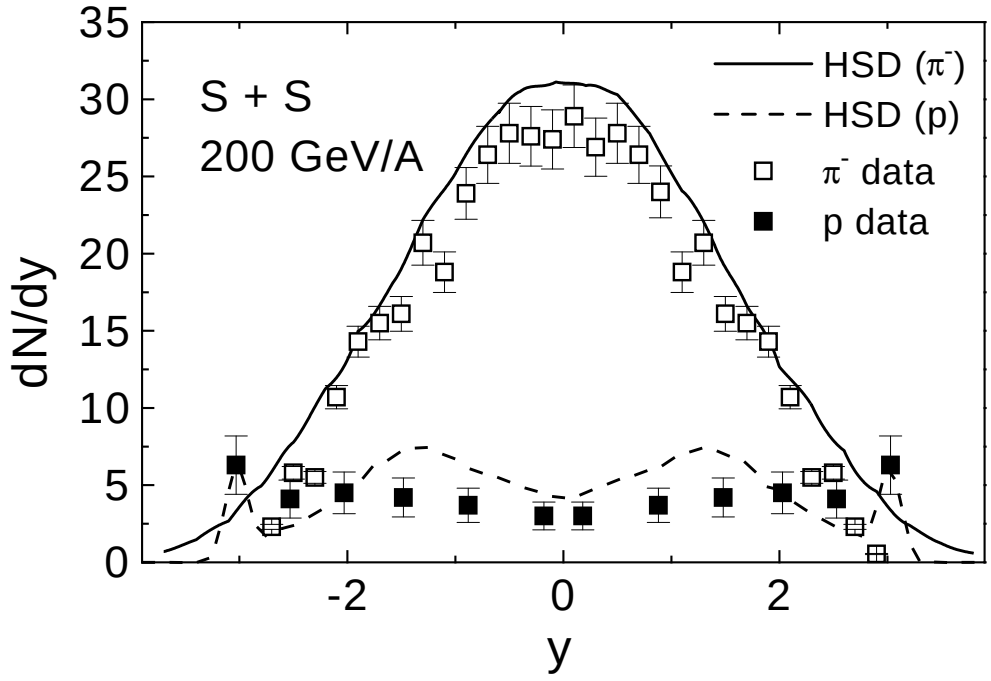

Fig. 20. Proton and π^- rapidity distribution for a central 200 GeV/A S + S collision in comparison to the data of ref. [65].

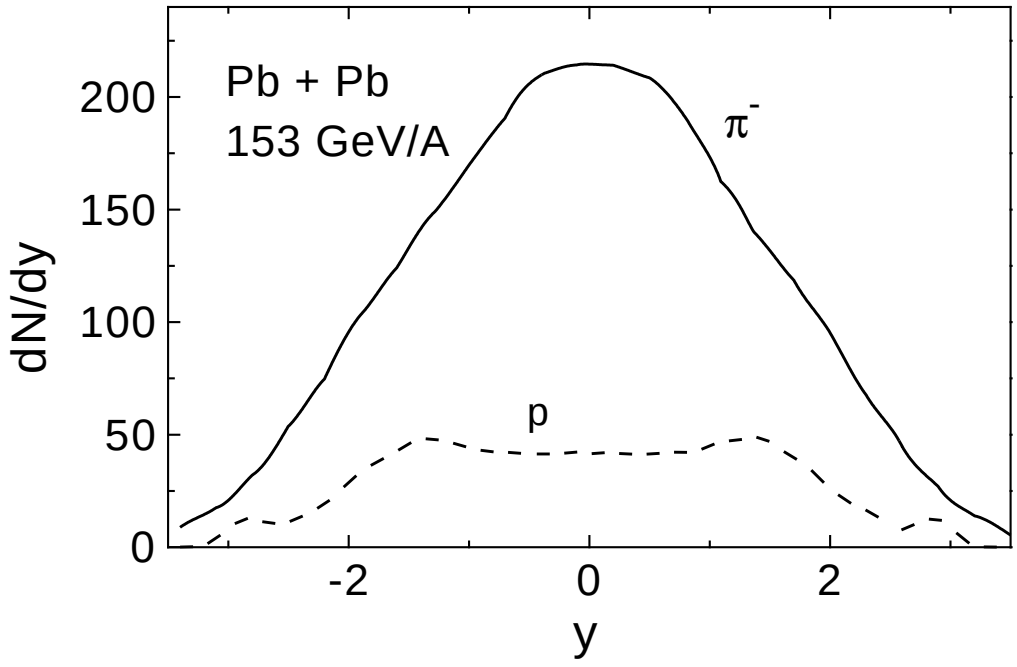

Fig. 21. Proton and π^- rapidity distribution for a 153 GeV/A Pb + Pb collision at b = 2 fm.

	exp.ratio	without kaon selfenergies	with kaon selfenergies
p + p	0.08	0.08	0.08
Si + Al	0.13	0.09	0.12
Si + Cu	0.16	0.1	0.15
Si + Au	0.19	0.11	0.16
Au + Au	0.22	0.12	0.21

Table 1. The K^+/π^+ ratio for p + p, Si + Al, Si + Au and Au + Au collisions at 14.6 GeV/A in comparison to the data from ref. [67].

seen experimentally. However, this enhancement could also be attributed to a closer approach to chemical equilibrium as advocated in ref. [67] which might be achieved due to enhanced hadronic cross sections in the dense medium. Whereas in principle the coupled transport equations (27) also describe the approach towards chemical equilibrium for large systems, it is not yet clear if the proper reactions rates are presently included in our simulations such that no final evidence on chiral symmetry restoration can be extracted so far.

The medium modifications of the ρ-meson are most efficiently probed by dilepton spectroscopy [54,56,62] since due to its short lifetime the ρ-meson has a good chance to decay in the dense baryonic environment. According to Fig. 14 we expect a substantial enhancement of dileptons in the invariant mass range 0.4 GeV $\leq$ M $\leq$ 0.7 GeV in nucleus-nucleus collisions as compared to p + A collsions due to a shift in the ρ-mass spectrum and an enhanced ρ-meson production in the dense medium especially via $\pi^+\pi^-$ annihilation [68,69]. In fact, first computations for dilepton production show that the enhancement of dileptons in central S + Au collisions at 200 GeV/A (reported by the CERES-collaboration [70]) might be explained by the chiral dynamics proposed in Section 4 [69].

6 Summary

In this work we have presented a relativistic transport approach (denoted by HSD [7]) where the underlying (real parts of) nucleon selfenergies have been determined from an effective NJL-type Lagrangian for the quark degrees of freedom with a chiral invariant interaction density. Starting with a local color current interaction we have developed a model for spin and isospin averaged

[7] Hadron-String-Dynamics

color neutral states on the basis of the experimental electromagnetic formfactor of the proton. The parameters in our model, which are all fixed by physical quantities are G_S and Λ_S for the scalar part, G_V and Λ_V for the vector part and α which describes the swelling of the nucleon in nuclear matter. The physical quantities, which are sufficiently well met are: The averaged nucleon mass M_N, the scalar vacuum condensate $\langle\bar{\psi}_q\psi_q\rangle$, the pion-nucleon Σ-term, the nuclear equation of state (minimum at $\rho = \rho_0$ with -16 MeV binding energy) and the Schroedinger equivalent potential U_{SEP} for nucleons. Due to the scalar-vector nature of the quark interaction density the nucleon selfenergies computed are also close to those of the σ-ω model of Walecka [23] in the low momentum and low density regime.

Whereas the real part of the nucleon selfenergies have been determined from a more microscopic approach, the imaginary part has been adopted from the LUND string fragmentation model [41] where the meson masses (except the pion) have been scaled in line with chirally invariant interaction densities. This more pragmatic model, of cause, has less founded reliability and thus one has to justify its applicability or inadequacy in comparison to experimental data.

As a first step in this direction we have applied our relativistic transport approach to nucleus-nucleus collisions from SIS to SPS energies. Whereas the proton and pion rapidity distributions look reasonable well for the systems studied experimentally, a clear signature for the chiral symmetry restoration could not unambiguously be established so far. This is because the strangeness enhancement observed experimentally at AGS and SPS energies might also be due to chemical equilibration or e.g. color-rope formation [55]. A better probe should be provided by dilepton spectroscopy in the invariant mass regime from 0.4 - 0.8 GeV [54] since the ρ-meson predominantly decays in the dense medium. In fact, first computations on e^+e^- production at SPS energies suggest that the dilepton enhancement seen by the CERES collaboration is due to partial chiral symmetry restoration [69].

The nuclear equation of state computed within our approach (Fig. 8) shows no density isomer up to $\rho \approx 10\rho_0$. This prediction is essentially due to the fact that scalar and vector baryon selfenergies are approximately of the same order of magnitude, but different sign, up to $\rho \approx 4\rho_0$ and the repulsive vector interaction takes over at even higher ρ together with the kinetic energy per nucleon. A density isomer thus can only occur if the vector coupling itself decreases at high baryon density or temperature. Some arguments in this direction have recently been proposed by Brown and Rho [71] and investigated in a model study by Li and Ko [72]. A clarification of this problem e.g. should be achieved by experimental data on the baryon flow as a function of projectile/target mass and bombarding energy in the energy regime in between SIS and SPS thus allowing for a closer look at the EOS at 'very high' baryon density.

The authors acknowledge valuable and inspiring discussions througout this work with C. M. Ko, U. Mosel, H. Stöcker, S. Teis and Gy. Wolf. They are also grateful to T. Maruyama for an earlier version of the relativistic transport code used in the analysis of nucleus-nucleus collisions in the energy regime below 1 GeV/A.

References

[1] W. Cassing and U. Mosel, Prog. Part. Nucl. Phys. 25 (1990) 235.

[2] B. Blättel, V. Koch and U. Mosel, Rep. Prog. Phys. 56 (1993) 1.

[3] S. Teis, W. Cassing, T. Maruyama, and U. Mosel, Phys. Lett. B319 (1993) 47; Phys. Rev. C50 (1994) 388.

[4] C. M. Ko, Q. Li and R. Wang, Phys. Rev. Lett. 59 (1987) 1084; C. M. Ko and Q. Li, Phys. Rev. C37 (1988) 2270; C. M. Ko, Nucl. Phys. A495

[5] X. S. Fang, C. M. Ko, G. Q. Li, and Y. M. Zheng, Phys. Rev. C49 (1994) R608; Nucl. Phys. A575 (1994) 766.

[6] G. Q. Li, C. M. Ko, X. S. Fang, and Y. M. Zheng, Phys. Rev. C49 (1994) 1139; G. Q. Li, C. M. Ko and X. S. Fang, Phys. Lett. B329 (1994) 149.

[7] K. Weber, B. Blättel, W. Cassing, H.-C. Dönges, V. Koch, A. Lang, and U. Mosel, Nucl. Phys. A539 (1992) 713.

[8] K. Weber, B. Blättel, W. Cassing, H.-C. Dönges, A. Lang, T. Maruyama, and U. Mosel, Nucl. Phys. A552 (1993) 571.

[9] T. Maruyama, W. Cassing, U. Mosel, S. Teis, and K. Weber, Nucl. Phys. A573 (1994) 653.

[10] J. Aichelin, Phys. Reports 202 (1991) 233; J. Aichelin and H. Stöcker, Phys. Lett. B176 (1986) 14; J. Aichelin, G. Peilert, A. Bohnet, A. Rosenhauer, H. Stöcker, and W. Greiner, Phys. Rev. C37 (1988) 2451.

[11] H. Sorge, H. Stöcker, and W. Greiner, Ann. Phys. 192 (1989) 266; Nucl. Phys. A498 (1989) 567c; H. Sorge, A. v. Keitz, R. Matiello, H. Stöcker, and W. Greiner, Z. Phys. C47 (1990) 629; Phys. Lett. B243 (1990) 7; A. Jahns, H. Sorge, H. Stöcker, and W. Greiner, Z. Phys. A341 (1992) 243.

[12] W. Botermans and R. Malfliet, Phys. Rep. 198 (1990) 115.

[13] R. Malfliet, Prog. Part. Nucl. Phys. 21 (1988) 207.

[14] G. E. Brown, Prog. Theor. Phys. 91 (1987) 85.

[15] G. E. Brown, C. M. Ko, Z. G. Wu, and L. H. Xia, Phys. Rev. C43 (1991) 1881.

[16] G. E. Brown and M. Rho, Phys. Rev. Lett. 66 (1991) 2720;

[17] V. Koch and G. E. Brown, Nucl. Phys. A560 (1993) 345.

[18] B. Peterson, Nucl. Phys. B30 (1992) 66.

[19] F. Karsch, Nucl. Phys. B34 (1993) 63.

[20] J. Engels, Phys. Lett. B252 (1990) 625; J. Engels, F. Karsch and K. Redlich, Nucl. Phys. B435 (1995) 295.

[21] F. Karsch and E. Laermann, Phys. Rev. D50 (1994) 6954.

[22] T. H. R. Skyrme, Phil. Mag. 1 (1956) 1043; Nucl. Phys. 9 (1959) 615.

[23] J. D. Walecka, Ann. Phys. 83 (1974) 491.

[24] B. D. Serot and J. D. Walecka, Adv. Nucl. Phys. vol. 16, ed. J. Negele and E. Vogt (Plenum, New York, 1986) p. 1

[25] U. Vogl and W. Weise, Prog. Part. Nucl. Phys. 27 (1991) 195.

[26] S. Klimt, M. Lutz, U. Vogl, and W. Weise, Nucl. Phys. A516 (1990) 429.

[27] U. Vogl, M. Lutz, S. Klimt and W. Weise, Nucl. Phys. A516 (1990) 469.

[28] M. C. Birse, J. Phys. G20 (1994) 1537.

[29] J. Hüfner, S. P. Klevansky, P. Zhuang and H. Voss, Ann. of Physics 234 (1994) 225.

[30] P. P. Domitrovich and H. Müther, J. Phys. G20 (1994) 1885.

[31] S. P. Klevansky, Rev. Mod. Phys. 64 (1992) 649

[32] T. Meissner, E. Ruiz Arriola and K. Goeke, Z. Phys. A339 (1990) 91.

[33] R. Alkhofer, H. Reinhardt and H. Weigel, preprint UNITU-THEP-25/1994, hep-ph/9412342, Dez. 1994.

[34] T. Meissner, E. Ruiz Arriola, A. Blotz and K. Goeke, preprint RUB-42/93.

[35] U. G. Meißner, Phys. Rep. 161 (1988) 213.

[36] V. Bernard, U.-G. Meißner, and A. A. Osipov, Phys. Lett. B324 (1994) 201.

[37] Y. Nambu and G. Jona-Lasinio, Phys. Rev. 122 (1961) 345; Phys. Rev. 124 (1961) 246.

[38] P. A. M. Guichon, Phys. Lett. B200 (1988) 235.

[39] K. Saito and A. W. Thomas, Phys. Rev. C51 (1995) 2757.

[40] M. Gell-Mann, R. Oakes, and B. Renner, Phys. Rev. 175 (1968) 2195.

[41] B. Nilsson-Almqvist and E. Stenlund, Comp. Phys. Comm. 43 (1987) 387.

[42] M. Gourdin, Phys. Rep. 11 (1974) 29; D. Krupa, S. Dubnicka, V. Kundrat, and V.A. Meshcheryakov, J. Phys. G10 (1984) 455.

[43] B. W. Bush and J. R. Nix, Ann. Phys. 227 (1993) 97.

[44] U. Kalmbach, T. Vetter, T. S. Biro, and U. Mosel, Nucl. Phys. A563 (1993) 584.

[45] T. Vetter, T. S. Biro and U. Mosel, Nucl. Phys. A581 (1995) 598.

[46] J. Gasser, H. Leutwyler and M. E. Sainio, Phys. Lett. B253 (1991) 252.

[47] T. D. Cohen, R. J. Furnstahl and D. K. Griegel, Phys. Rev. C45 (1992) 1881.

[48] F. E. Close, R.L. Jaffe, R.G. Roberts, and G.G. Ross, Phys. Rev. D31 (1985) 1004.

[49] S. Hama, B. C. Clark, E. D. Cooper, H. S. Sherif and R. L. Mercer, Phys. Rev. C41 (1990) 2737.

[50] R. D. Bowler and M. C. Birse, Nucl. Phys. A582 (1995) 655.

[51] R. Machleidt, K. Holinde and Ch. Elster, Phys. Rep. 149 (1987) 1.

[52] R. Brockmann and W. Weise, in 'Hadrons in Nuclear Matter', Proceedings of the International Workshop XXIII on Gross Properties of Nuclei and Nuclear Excitations, Hirschegg, Austria, Jan. 1995, ed. by H. Feldmeier and W. Nörenberg, p. 12.

[53] G. Q. Li and C. M. Ko, Phys. Lett. B338 (1994) 118.

[54] Gy. Wolf, W. Cassing, W. Ehehalt, and U. Mosel, Prog. Part. Nucl. Phys. 30 (1993) 273.

[55] H. Sorge, private communication.

[56] C. M. Ko, Nucl. Phys. A583 (1995) 591c.

[57] D. B. Kaplan and A. E. Nelson, Phys. Lett. B175 (1986) 57.

[58] T. Hatsuda and S. H. Lee, Phys. Rev. C46 (1992) R34.

[59] K. Niita, W. Cassing and U. Mosel, Nucl. Phys. A504 (1989) 391.

[60] Gy. Wolf, G. Batko, W. Cassing, U. Mosel, K. Niita, and M. Schäfer, Nucl. Phys. A517 (1990) 615.

[61] F.D. Berg et al., Phys. Rev. Lett. 72 (1994) 977.

[62] W. Ehehalt, W. Cassing, A. Engel, U. Mosel, and Gy. Wolf, Phys. Lett. B298 (1993) 31.

[63] T. Abbott et al., E802 Coll., Phys. Rev. C50 (1994) 1024.

[64] P. Braun-Munzinger, private communication.

[65] H. Stroebele et al., Nucl. Phys. A525 (1991) 59c.

[66] M. Gyulassy, Quark Matter 95, preprint CU-TP-685.

[67] P. Braun-Munzinger, J. Stachel, J.P. Wessels, and N. Xu, Phys. Lett. B344 (1995) 43.

[68] G.Q. Li, C.M. Ko, and G.E. Brown, submitted to Phys. Rev. Lett.

[69] W. Cassing, C.M. Ko, and W. Ehehalt, to be published.

[70] A. Drees, in 'Hadrons in Nuclear Matter', Proceedings of the International Workshop XXIII on Gross Properties of Nuclei and Nuclear Excitations, Hirschegg, Austria, Jan. 1995, ed. by H. Feldmeier and W. Nörenberg, p. 151.

[71] G.E. Brown and M. Rho, Phys. Lett. B338 (1994) 301.

[72] G. Q. Li and C. M. Ko, Phys. Lett. B351 (1995) 37.